Proceedings of the
Annual Stability Conference
Structural Stability Research Council
Orlando, Florida, April 12-15, 2016

Local-Distortional-Global Interaction in Cold-Formed Steel Lipped Channel Columns: Behavior, Strength and DSM Design

Pedro B. Dinis[1], Ben Young[2], Dinar Camotim[1]

Abstract

This work deals with the structural behavior and ultimate strength of fixed-ended cold-formed steel (CFS) lipped channel columns experiencing various levels of local-distortional-global (L-D-G) mode interaction. Initially, the paper addresses the selection of the column cross-section dimensions and lengths, intended to ensure various L-D-G interaction levels (more or less close critical stresses). Then, attention is turned to the experimental test campaign carried out at The University of Hong Kong, aimed at (i) providing experimental evidence and characterization of the occurrence of L-D-G interaction, and (ii) quantifying the associated failure load erosion. Next, the test results are used to develop and validate an ABAQUS non-linear shell finite element model, subsequently employed to perform a parametric study that is mostly intended to gather (numerical) failure load data − 368 fixed-ended columns exhibiting different geometries and various yield stresses, which ensure covering a wide slenderness range. Finally, the paper also assesses the quality of the failure load estimates provided by various design approaches, based on the Direct Strength Method (DSM), for CFS columns affected by the triple coupling phenomenon under consideration. This assessment is based on the comparison with both (i) the experimental and numerical failure loads obtained in this work, and (ii) additional ultimate strength values collected from the literature.

1. Introduction

Thin-walled cold-formed steel (CFS) lipped channel columns are known to be highly prone to several instability phenomena, namely local (L), distortional (D) and global (G − flexural or flexural-torsional) buckling − Figs. 1(b)-(d) depict the corresponding lipped channel cross-section buckled shapes. Depending on the column geometry and end support conditions, the column post-buckling behavior and strength may be significantly eroded by the interaction between these three buckling mode types.

Out of the above interaction phenomena, the one stemming from the nearly simultaneous occurrence of local and global buckling is the better understood − its effects are already taken into account by all steel design codes, using either the traditional Effective Width Method or the more recent Direct Strength Method (DSM). In the last decade, considerable research work has been devoted to local-distortional (L-D) interaction, including experimental investigations, numerical simulations and proposals of DSM-based design approaches (*e.g.*, Yang & Hancock 2004, Dinis *et al.* 2007, Kwon *et al.* 2009, Silvestre *et al.*

[1] CERIS, ICIST, DECivil, Instituto Superior Técnico, Universidade de Lisbon, Portugal. <dinis; dcamotim@civil.ist.utl.pt>
[2] Department of Civil Engineering, The University of Hong Kong, Hong Kong, China. <young@hku.hk>

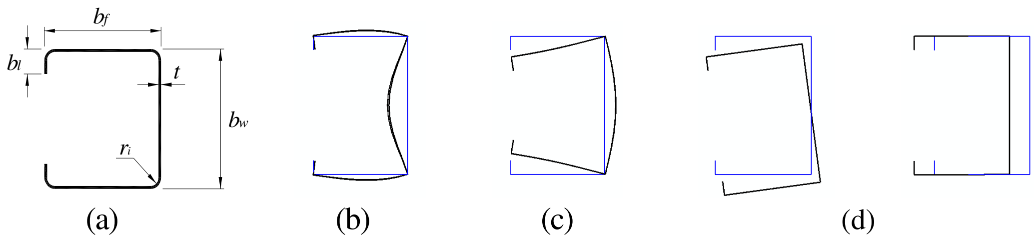

Figure 1: Lipped channel (a) geometry and cross-section deformed shapes associated with column (b) local, (c) distortional and (d) global (flexural-torsional and flexural) buckling

2012, Young *et al.* 2013a, Martins *et al.* 2015a) – this research work showed that the column ultimate strength is bound to be affected by the coupling between these two buckling modes, either (i) when the critical local and distortional buckling loads are close (ratio between 0.9 and 1.1 – "true interaction"), or (ii) when the local critical buckling stress is considerably lower than its distortional counterpart, provided that the yield stress exceeds the distortional critical buckling stress by a "large enough" amount ("secondary distortional bifurcation interaction") (Martins *et al.* 2015b). Concerning coupling phenomena involving distortional and global buckling, namely distortional-global (D-G) and local-distortional-global (L-D-G) interaction, the available literature is much scarcer. In the latter case, research work has been reported by Young & Yan (2002), Dinis & Camotim (2011), Dinis *et al.* (2011, 2012, 2014), Santos *et al.* (2012, 2014a,b), Young *et al.* (2013b), Cava (2015), and Cava *et al.* (2015), but no more than incipient design considerations are available. Thus, it is fair to say that a systematic investigation addressing the behavior of CFS columns undergoing different levels of L-D-G interaction are still missing – the present work, involving both experimental tests and numerical simulations, aims at contributing towards filling this gap.

The paper begins by presenting and discussing the selection of the nominal cross-section dimensions and lengths of the CFS lipped channel columns undergoing L-D-G mode interaction intended to be tested – the column geometries are carefully selected to ensure various levels of interaction (more or less close critical loads). The column selection is carried out by means of Generalized Beam Theory (GBT) buckling analyses, performed with code GBTUL (Bebiano *et al.* 2008a,b), and the columns selected exhibit (i) critical local (P_{crL}) or distortional (P_{crD}) loads (*i.e.*, $P_{cr.min}$=P_{crL} or P_{crD}), and (ii) different load ratios $P_{cr.max}/P_{cr.min}$ and $P_y/P_{cr.max}$, where $P_{cr.max}=max(P_{crL};P_{crD};P_{crG})$, P_{crG} is the global (flexural-torsional) buckling load and P_y the squash load – when the three buckling loads are not very close, the development of L-D-G interaction effects is also governed by the closeness between P_y and $P_{cr.max}$. Then, the paper presents the most relevant results of an experimental investigation carried out at The University of Hong Kong (UHK), aimed at assessing the non-linear (post-buckling) behavior and ultimate strength of fixed-ended CFS lipped channel columns with load ratios $1.39 \geq P_{cr.max}/P_{cr.min} \geq 1.11$ and $3.04 \geq P_y/P_{cr.max} \geq 1.43$. This experimental study, fully reported by Young *et al.* (2015), provides (i) clear evidence of the occurrence of L-D-G interaction and (ii) the means to validate a previously developed shell finite element model, which is subsequently employed to obtain failure load data that are essential for the development, calibration and validation of a DSM-based design approach for columns failing in L-D-G interactive modes – numerical simulations of three UHK experimental tests, carried out by means of ABAQUS shell finite element analyses (SFEA), are presented and discussed. Then, this SFE model is employed to carry out a parametric study aimed at gathering additional numerical failure load data to help developing a DSM-based design approach for lipped channel columns undergoing triple interaction. The columns analyzed in this work exhibit either (i) the geometries of the specimens tested at UHK or (ii) the cross-section dimensions recently identified by Cava (2015). The tested specimens exhibit (i) mostly critical local buckling loads and (ii) critical L-D-G buckling loads such that $1.39 \geq P_{cr.max}/P_{cr.min} \geq 1.11$. On the other hand, the columns selected by Cava (2015) exhibit critical buckling loads no more than 30% apart ($1.27 \geq P_{cr.max}/P_{cr.min} \geq 1.04$) and ordered in all possible sequences – the ratios P_{crD}/P_{crL}, P_{crgG}/P_{crD} and P_{crG}/P_{crL} are always comprised between 0.8 and 1.2. Finally, the experimental and numerical failure loads reported in this paper, as well as others collected from the available literature (the numerical failure loads are gathered from previous publications by the authors), are used to draw fairly definite conclusions concerning the establishment of a DSM-based design approach that can handle efficiently (accurately, safely and reliably) triple interactive failures in CFS lipped channel columns – a total of 52 experimental and 893 numerical failure loads are considered for this purpose.

2. Buckling Behavior – Column Geometry Selection

In order to obtain lipped channel column geometries (web width b_w, flange width b_f, stiffener width b_s, wall thickness t and length L – see Fig. 1(a)) ensuring various levels of interaction effects (more or less close critical P_{crL}, P_{crD}, P_{crG} loads), it was necessary to perform sequences of "educated" trial-and-error buckling analyses by means of code GBTUL (Bebiano *et al.* 2008a,b), mainly due to its computational efficiency and modal nature, taking into account that the specimens would be manufactured from a high strength zinc-coated structural steel sheet with nominal thickness 1.00 and 1.20 mm. The first step of the procedure consists of identifying column geometries ensuring nearly coincident local, distortional and global critical buckling loads (*i.e.*, $P_{crL} \approx P_{crD} \approx P_{crG}$) – the rounded corners are disregarded, since their influence has been found to be negligible. Then, it is possible to select the level of interaction between the three buckling modes by slightly changing the member dimensions (*e.g*, web/flange width or length). In this investigation, it was decided to select mostly columns with (i) critical local loads (*i.e.*, $P_{cr.min}=P_{crL}$), (ii) $P_{cr.max}/P_{cr.min}>1.1$, where $P_{cr.max}=max\,(P_{crL}; P_{crD}; P_{crG})$, and (iii) $P_y/P_{cr.max}>1.4$, to allow for the development of triple interaction prior to collapse – the end product of this trial-and-error procedure is given in Table 1 (included in Section 3).

In order to illustrate the concepts involved in the column geometry selection, Fig. 2(a) depicts two curves providing the variation of the critical buckling load P_{cr} with the length L (logarithmic scale), concerning columns with cross-section dimensions (i) b_w=75 mm, b_f=65 mm, b_s=12 mm, t=1.2 mm (C1 column), and (ii) b_w=78 mm, b_f=68 mm, b_s=12.5 mm, t=1.2 mm (C2 column – 4% higher web, flange and stiffener widths stemming, for instance, from a manufacture inaccuracy). The comparative analysis of these two buckling curves prompts the following remarks:

(i) The C1 column P_{cr} vs. L curve exhibits three zones, corresponding to local buckling (L<120 cm), local-distortional "mixed" buckling (almost horizontal plateau associated with very close buckling loads corresponding to local-distortional modes with various half-wave numbers) (120<L<210cm), and global (flexural-torsional) buckling (L>210 cm).

(ii) Fig. 2(a) clearly shows that the C1 column with L=210 cm has nearly coincident L, D and G critical loads ($P_{cr.max}/P_{cr.min}$=1.05): $P_{cr.D}$=63.9kN (4 distortional half-waves), $P_{cr.L}$=64.2kN (33 web-triggered local half-waves) and $P_{cr.G}$=67.4kN (single flexural-torsional half-wave) – the corresponding buckling mode shapes are depicted in Fig. 2(b). This means that this column post-buckling behavior and failure load will be highly affected by L-D-G interaction ($L \equiv L_{L/D/G}$). Columns with lengths below or above $L_{L/D/G}$ exhibit $P_{crG}>P_{crL} \approx P_{crD}$ or $P_{crG}<P_{crL} \approx P_{crD}$, respectively – note that $P_{cr.max}/P_{cr.min}$ increases from 1.05 ($L_{L/D/G}$) to 1.10 (L=190 cm) and 1.20 (L=230 cm).

(iii) Obviously, the buckling behaviors of the C2 and C1 columns are similar. However, due to the slightly higher cross-section dimensions, the $P_{cr.max}/P_{cr.min}$ of the C2 column with L=210 cm is 1.18 (instead of 1.05, value of the C1 column).

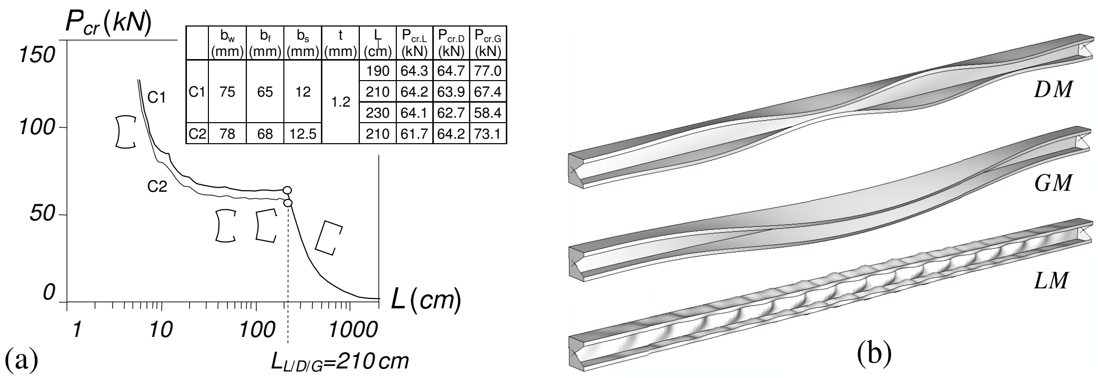

	b_w (mm)	b_f (mm)	b_s (mm)	t (mm)	L (cm)	$P_{cr.L}$ (kN)	$P_{cr.D}$ (kN)	$P_{cr.G}$ (kN)
C1	75	65	12	1.2	190	64.3	64.7	77.0
					210	64.2	63.9	67.4
					230	64.1	62.7	58.4
C2	78	68	12.5		210	61.7	64.2	73.1

Figure 2: (a) C1 and C2 column P_{cr} vs. L curves and (b) $L_{L/D/G}$ C1 column distortional, global (flexural-torsional) and local buckling mode shapes

2.1 Types of Interaction

As mentioned before, L-D-G interaction may occur in members exhibiting geometries (cross-section shape and dimensions, and length) such that either (i) the local, distortional and global critical buckling loads are very close (P_{crL}≈P_{crD}≈P_{crG} – the criterion adopted is that $P_{cr.max}/P_{cr.min}$≤1.10, where $P_{cr.max}$ and $P_{cr.min}$ are the largest and smallest of the above three critical buckling loads), which characterizes the so-called "true L-D-G-interaction", or (ii) the local and/or distortional critical buckling loads are visibly lower than the remaining one(s), provided that the squash load P_y exceeds the highest critical buckling load by a large enough amount (*i.e.*, $P_y>P_{cr.max}$), which characterizes the so-called "secondary bifurcation L-D-G interaction". It is worth noting that, as shown by Dinis *et al.* (2012), no L-D-G interaction occurs when the global critical buckling loads is visibly lower than their local and distortional counterparts – this is because of the very small post-critical strength reserve associated with global buckling, which precludes reaching applied loads close to the critical local and/or distortional buckling loads. Naturally, the most pronounced "secondary bifurcation L-D-G interaction" occurs when the lowest critical buckling load is local, due to the large post-critical strength reserve – if $P_{cr.min}=P_{crD}$ the post-critical strength reserve is just moderate.

In order to provide a better grasp of the difference between the two L-D-G interaction types mentioned above, Figs. 3(a)-(b) display the elastic equilibrium paths and six cross-section buckled configurations concerning lipped channel columns exhibiting "true L-D-G-interaction" and "secondary distortional/global bifurcation L-D-G interaction", respectively – the latter corresponds to a situation in which $P_{cr.min}=P_{crL}$ and $P_{cr.max}=P_{crD}\approx P_{crG}$. In the first case, coupling starts at the early loading stages and evolves as loading progresses – local, distortional and global (flexural-torsional) deformations develop along the whole equilibrium path, provided that the column contains initial geometrical imperfections with L, D and G

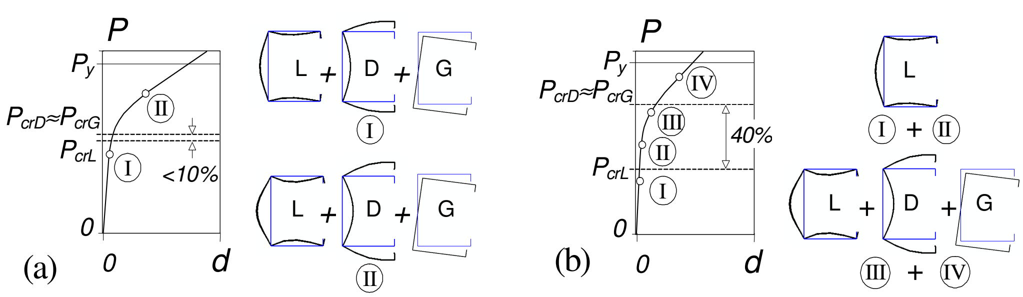

Figure 3: Equilibrium paths and cross-section buckled shapes of lipped channel columns exhibiting (a) true and (b) secondary distortional/global bifurcation L-D-G interaction

components. In the second case, on the other hand, the deformation is essentially local until the vicinity of the critical distortional/global buckling load level, when visible distortional and global deformations begin to emerge and subsequently develop – of course, this is only possible if P_y is “high enough” to allow for this emergence and/or development (otherwise, plasticity kicks in and precipitates a local failure prior to the emergence of the distortional and global deformations).

3. Experimental Investigation

This section addresses the experimental investigation carried out at The University of Hong Kong and fully reported in Young *et al.* (2015). The CFS lipped channel column specimens were brake-pressed from high strength zinc-coated structural steel sheets of grades G500 and G550 – the nominal thickness and yield stress are (i) t=1.2mm and f_y=500MPa (G500) and (ii) t=1.0mm and f_y=550MPa (G550). All measured specimen cross-section dimensions and lengths are given in Table 1, together with the associated column critical buckling loads (E=210GPa and ν=0.3) and squash load (P_y=Af_y, where the areas A were computed on the basis of the average measured cross-section dimensions – the rounded corners were disregarded): eight specimens with t=1.0mm, labeled LC1-4, LC9-12, and eight specimens with t=1.2mm, labeled LC5-8, LC13-16 – to check the test repeatability, two nearly identical LC2 specimens were tested. The inside corner radius was 2.0mm in all cases and the specimen end sections were welded to 25mm thick steel end plates, ensuring full contact with the test machine end bearings (fixed end supports) – see Fig. 4(a).

The material properties of the column specimens were determined by means of tensile coupon tests – the coupons were extracted from the centre of the flange and web, in the longitudinal direction, of specimens LC-1 and LC-5. The CFS lipped channel column specimens were fabricated from the same batch of steel, for each wall thickness. Therefore, the material properties obtained from specimens LC-1 and LC-5 are

Table 1: Column specimen (i) geometries, (ii) squash and critical (local, distortional, global) buckling loads, and (iii) load ratios, (iv) initial geometrical imperfection amplitudes, (v) experimental failure loads and (vi) observed failure mode natures

Column specimens	b_w (mm)	b_f (mm)	b_s (mm)	t^* (mm)	L (mm)	P_y (kN)	P_{crL} (kN)	P_{crD} (kN)	P_{crG} (kN)	$\frac{P_{cr.int}}{P_{cr.min}}$	$\frac{P_{cr.max}}{P_{cr.min}}$	$\frac{P_y}{P_{cr.min}}$	Δ_0 (mm)	δ_0/L	P_{Exp} (kN)	Failure mode
LC1	53.5	56.7	12.5	0.985	1395	104.0	47.6	56.6	58.3	1.19	1.23	1.94	0.945	1/4394	46.15	L+D+FT
LC2-1	57.5	61.4	12.4	0.997	1651	112.5	45.2	51.7	51.6	1.14	1.14	2.38	0.575	–1/32503	44.78	L+D+FT
LC2-2	57.6	61.4	12.5	1.001	1649	113.1	45.7	52.9	52.9	1.16	1.16	2.33	0.575	–1/66891	44.20	L+D+FT
LC3	62.6	66.2	12.5	1.001	1951	121.1	42.0	46.4	46.0	1.10	1.11	2.85	0.385	–1/4043	39.83	L+D+FT
LC4	68.7	71.0	12.5	0.976	2300	126.5	35.7	40.4	40.5	1.13	1.13	3.41	0.805	–1/12075	39.68	L+D+FT
LC5	70.8	72.3	12.2	1.193	1896	143.0	63.2	59.4	69.7	1.06	1.17	2.46	–0.175	1/29860	61.67	L+D+FT
LC6	70.9	78.3	11.9	1.203	2004	151.2	60.3	54.2	64.0	1.11	1.18	2.84	0.108	–1/3586	59.19	L+D+FT
LC7	75.7	82.9	12.0	1.194	2302	158.5	55.3	50.2	59.0	1.10	1.18	3.22	–0.865	–1/1888	49.49	L+D+FT
LC8	82.1	87.7	11.8	1.171	2603	164.6	48.7	43.7	54.8	1.11	1.25	3.61	–1.780	–1/2927	47.46	L+D+FT
LC9	58.0	48.2	12.8	0.983	1401	97.3	47.6	63.8	65.4	1.34	1.37	1.62	0.260	–1/4596	51.13	L+D+FT
LC10	63.3	52.6	12.7	0.989	1602	105.5	43.9	57.4	61.2	1.31	1.39	1.88	0.105	1/15769	50.55	L+D+FT
LC11	62.7	63.9	12.4	0.987	1699	116.9	41.2	48.2	53.7	1.17	1.30	2.37	0.475	–1/66891	42.59	L+D+FT
LC12	68.5	57.3	12.8	0.986	1899	113.2	39.8	51.7	53.9	1.30	1.35	2.29	–0.050	–1/6501	46.24	L+D+FT
LC13	73.2	63.3	12.4	1.204	1851	135.2	67.0	69.1	78.9	1.03	1.18	2.06	–0.208	–1/2974	66.82	L+D+FT
LC14	78.4	68.4	12.5	1.174	2100	141.0	57.5	60.9	71.3	1.06	1.24	2.37	–1.238	–1/2756	60.74	L+D+FT
LC15	83.3	73.4	11.9	1.176	2402	149.3	53.7	53.0	64.1	1.01	1.21	2.79	0.733	–1/4202	55.47	L+D+FT
LC16	88.5	78.3	12.3	1.204	2750	162.4	54.0	53.0	61.5	1.02	1.16	3.17	–0.735	–1/10826	52.06	L+D+FT

expected to apply also to the other specimens having the same nominal wall thickness. For the LC1 and LC5 specimens, the measured Young's modulus and 0.2% proof stress were (i) E_0=211-218GPa + $\sigma_{0.2}$=597-612MPa (G550 steel) and (ii) E_0=213-215GPa + $\sigma_{0.2}$=594-598MPa (G500 steel) – higher E_0 and $\sigma_{0.2}$ values for the web coupons. Fig. 4(b) shows the stress-strain curves of two specimen tensile coupon tests – note that the steel exhibits practically no strain-hardening.

To assess the specimen initial configuration, two displacements were measured at mid-height prior to testing: Δ_0 and δ_0 (see Fig. 4(d)) – all measured Δ_0 and δ_0 values are given in Table 1, with the latter normalized with respect to the column length L. The Δ_0 values concern the initial distortional deformation and correspond to half the difference between the distances, measured parallel to the web, between the flange-stiffener and web-flange corners (positive Δ_0 means outward flange-stiffener motions) – the maximum Δ_0 measured was 1.78mm (LC8). The δ_0 values may stem from various combinations of initial (i) minor-axis flexure, (ii) torsional rotation (recall the shear center location) and, to a lesser extent (δ_0 is measured close to a web-flange corner), (iii) local and/or distortional deformations (both cause web transverse bending) – the maximum δ_0/L measured was 1/1888 (LC7). Note that (i) positive δ_0/L values stand for minor-axis bending curvatures towards the lips and (ii) initial displacement profiles were not measured, *i.e.*, no knowledge about the initial imperfection longitudinal shape is available.

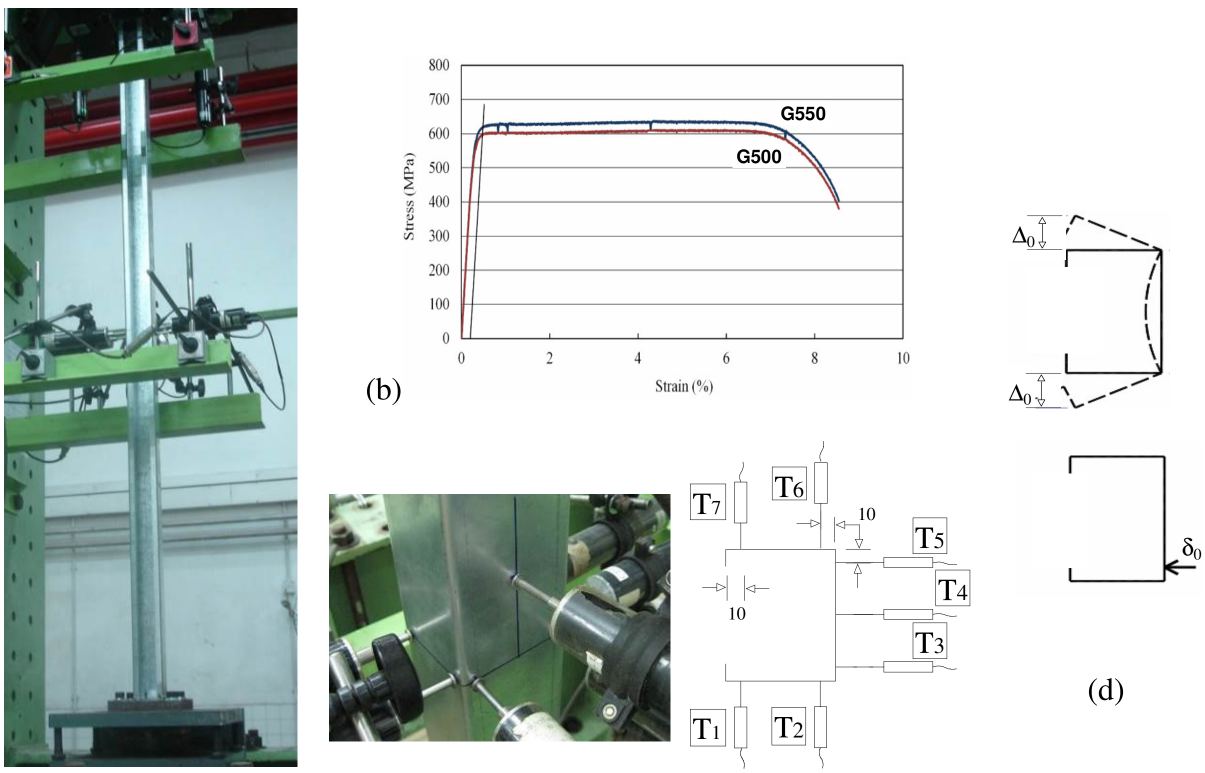

(a) (c)

Figure 4: (a) Fixed-ended column test set-up, (b) coupon stress-strain curves, (c) location of the displacement transducers (mid-height cross-section), and (d) mid-height initial displacement measurements

3.1 Test Results

Since the 17 column specimens tested shared essentially the same structural response, only a representative sample of the (i) recorded equilibrium paths and (ii) observed deformed configurations (including failure modes) are presented.

The experimental failure loads obtained are given in Table 1, together with the observed failure mode natures – Figs. 5(a)-(b) show the deformed configurations near collapse of specimens LC7 and LC13. As for Fig. 5(c), it depicts the applied load vs. axial shortening equilibrium path of specimen LC5 – several other equilibrium paths, corresponding to other specimens and transducer measurements, were recorded and reported by Young *et al.* (2015).The analysis of these experimental results prompts the following remarks:

(i) All specimens failed in local-distortional-global (flexural-torsional) interactive modes ("L+D+FT") – Fig. 5(a)-(b) show the deformed configurations near collapse of specimens LC7 and LC13, clearly evidencing the simultaneous occurrence of local, distortional and flexural-torsional deformations.

(ii) However, the local, distortional and flexural-torsion deformations observed do not stem from the near coincidence of the L, D and G column critical buckling loads – Table 1 shows that the ratio between the highest and lowest buckling loads varies between 1.16 and 1.39 for all the columns. Instead, the interaction occurs because (ii_1) the squash load (*i.e.*, the yield stress) is "sufficiently larger" than the highest column buckling load (the corresponding ratio varies between 1.61 and 3.37) and (ii_2) global buckling is never critical – numerical studies showed that such columns fail in "pure" global modes, without the occurrence of visible interaction with L or D buckling (Dinis *et al.* 2012).

(iii) The ultimate strengths corresponding to the repeated tested specimens exhibiting L-D-G interaction (specimens LC-2-1 and LC-2-2) differed by 1.3%, thus evidencing quite good test repeatability.

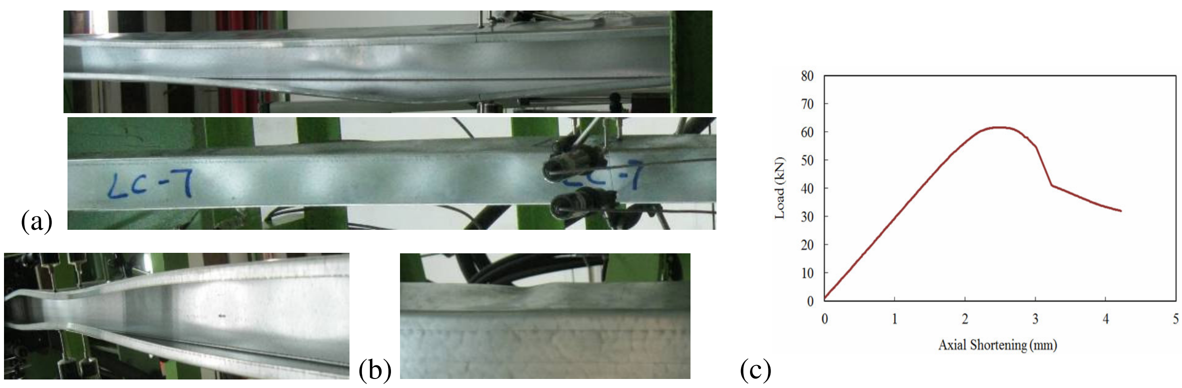

Figure 5: Experimental evidence of local-distortional-global interaction in specimens (a) LC7 and (b) LC13 (front and back views), and (c) load vs. axial shortening curve concerning specimen LC5

4. Numerical Simulations

This section deals with the numerical simulation of some of the experimental tests by means of ABAQUS shell finite element analyses (SFEA). The analyses carried out (i) adopt column discretizations into fine meshes of S4 elements (ABAQUS nomenclature: 4-node isoparametric elements) with length-to-width close to 1, and (ii) model the column supports by attaching rigid plates to their end section centroids. The numerical results presented, discussed and compared with the corresponding experimental values concern the non-linear behavior, ultimate strength and collapse of specimens LC2-1, LC8 and LC12. It is important to begin by stating the assumptions adopted to perform the numerical simulations:

(i) The steel exhibits an elastic-plastic isotropic behavior characterized by E and f_y values taken as the lowest ones obtained/measured from the tensile coupon tests – it is always assumed that ν=0.3. Such values were E=211 GPa + f_y=597 MPa (G550) and E=213 GPa + f_y=594 MPa (G500), respectively for specimens LC2-1+LC12 and LC8. Moreover, the steel material behavior is described by a multi-linear model that approximates quite closely the experimentally obtained stress-strain curve prior to the yield plateau: linear segments connecting the points concerning stresses f=0.75f_y, 0.90f_y, 0.98f_y and f_y – Fig. 6 compares the experimental curve for G550 steel with its multi-linear approximation adopted in the numerical simulations.

(ii) The column support conditions are fully fixed except for the axial displacement of the loaded end section, which is completely free.

(iii) Both residual stresses (not measured in the tested specimens) and rounded corner effects are neglected – in cold-formed steel members, such effects have been shown to have a fairly small combined impact on the column failure load (Ellobody & Young 2005).

(iv) The initial geometrical imperfections considered, which are intended to replicate the test specimen deformed configurations (measured prior to testing), combine two buckling modes, namely (iv$_1$) the critical distortional (D) mode with several half-waves and (iv$_2$) a single half-wave flexural-torsional (FT) or minor-axis flexural (F) mode – the amplitudes of these modes are the Δ_0 and δ_0 values shown in Fig. 4(d), obtained from the measurements of the displacement transducers indicated in Fig. 4(c). These values are (iv$_1$) Δ_0=+0.575 mm and δ_0=−0.051 mm (specimen LC2-1), (iv$_2$) Δ_0=−1.780 mm and δ_0=−0.889 mm (specimen LC8), and (iv$_3$) Δ_0=−0.050 mm and δ_0=−0.292 mm (specimen LC12).

(v) Each column was analyzed with several initial geometrical imperfections, namely (v$_1$) pure distortional (N$_1$), flexural-torsional (N$_2$) and flexural (N$_3$) imperfections, and (v$_2$) combined distortional+flexural-torsional (N$_4$) and distortional+flexural (N$_5$) imperfections.

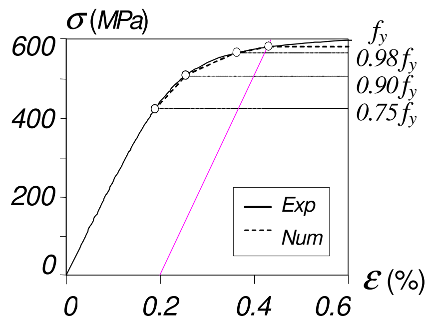

Figure 6: Experimentally measured stress-strain curve and multi-linear approximation

Figs. 7(a), 8(a) and 9(a) show the LC2-1, LC8 and LC12 specimen numerical and experimental equilibrium paths (i) P *vs.* d_1 and P *vs.* d_7 (d_1 and d_7 are the measurements of transducers 1 and 7 shown in Fig. 4(c) – inward displacements are positive), and (ii) P *vs.* ε, where ε is the column axial shortening. The numerical results concern columns containing N$_1$-N$_5$ (LC2-1 specimen) or N$_4$ (LC8 and LC12 specimens) initial imperfections and Table 2 provides the corresponding failure loads (P_{Num}) – this table also provides the numerical failure loads of columns with the LC8 and LC12 specimen geometry containing all N$_1$-N$_5$ initial geometrical imperfections. On the other hand, Fig. 7(b), 8(b) and 9(b) display views of the specimen failure mode configurations (deformed configurations at the onset of collapse) observed experimentally (front and back views) and obtained numerically for the N$_4$ imperfection (including the plastic strains and a zoom view of the top flange, showing local deformations). The observation and comparative analysis of all these numerical and experimental results leads to the following comments:

(i) There is a very good correlation between the three sets of failure mode representations shown in Figs. 7(b), 8(b) and 9(b), both providing experimental and numerical evidence of the occurrence of L-D-G interaction. Notice the local deformations clearly visible in the back views of the LC2-1, LC8

Table 2: LC2-1, LC8 and LC12 specimen (i) initial geometrical imperfection amplitudes, (ii) numerical failure loads (P_{Num}) and (iii) experimental failure loads (P_{Exp})

	Specimen LC2-1					Specimen LC8					Specimen LC12				
SFEA	Imperfection					Imperfection					Imperfection				
Mode	N1	N2	N3	N4	N5	N1	N2	N3	N4	N5	N1	N2	N3	N4	N5
D	Δ_0	–	–	Δ_0	Δ_0	Δ_0	–	–	Δ_0	Δ_0	Δ_0	–	–	Δ_0	Δ_0
FT	–	δ_0	–	δ_0	–	–	δ_0	–	δ_0	–	–	δ_0	–	δ_0	–
F	–	–	δ_0	–	δ_0	–	–	δ_0	–	δ_0	–	–	δ_0	–	δ_0
P_{Num} (kN)	52.03	47.24	48.26	45.19	46.62	56.65	49.70	51.68	49.05	50.69	55.35	46.58	46.83	45.89	45.83
P_{Exp} (kN)	44.75					47.46					46.24				

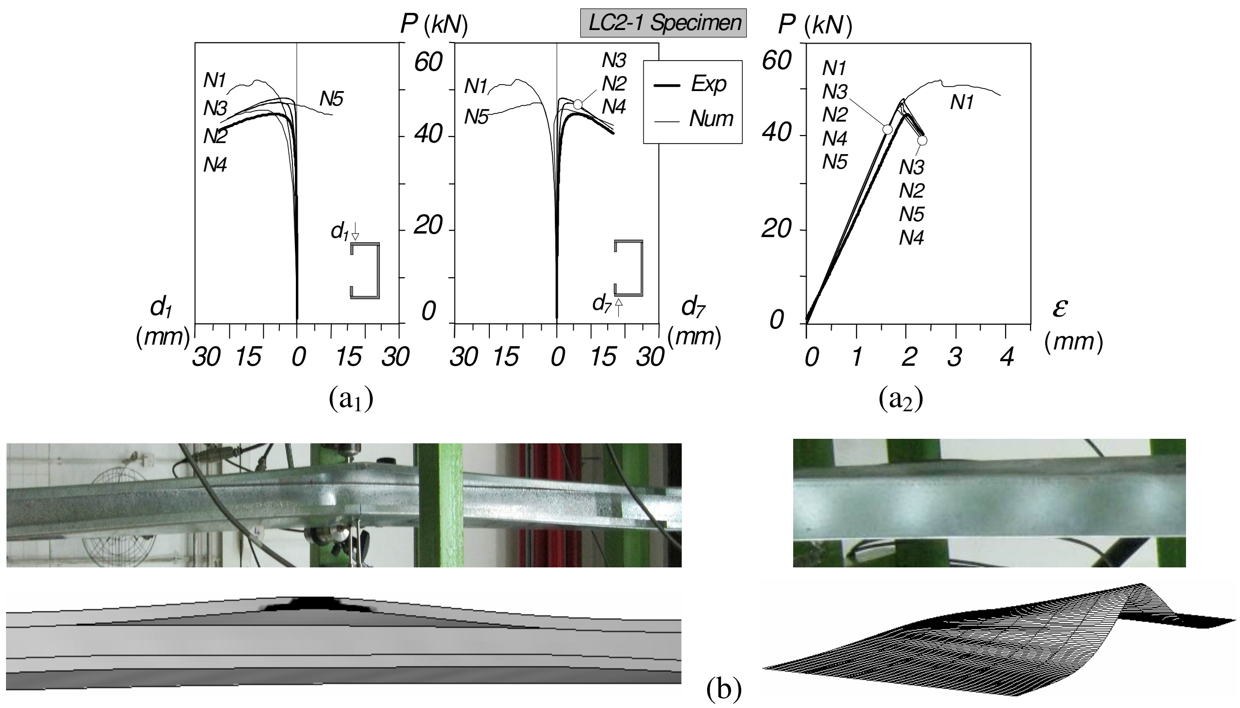

Figure 7: LC2-1 specimen (a) numerical (N1-N5) and experimental P vs. d_1, P vs. d_7 and P vs. ε equilibrium paths, and (b) experimental (front and back views) and numerical (N4 – front and top flange views) failure modes

and LC12 specimen failure modes, a feature that was not observed in the experimental investigations reported by Santos *et al.* (2012, 2014a), concerning columns with close L, D, G critical buckling loads ($1.00 \leq P_{cr.max}/P_{cr.min} \leq 1.10$) and $P_y/P_{cr.max}$ values in the 1.16-2.13 range – this issue will be further addressed later.

(ii) The L-D-G mode interaction occurs even when the three critical buckling loads are not very close – recall that the LC2-1, LC8 and LC12 specimen $P_{cr.max}/P_{cr.min}$ values are 1.14, 1.11 and 1.35, respectively. This is because P_{crL} is the lowest critical buckling load (high post-critical strength) and the yield stress is considerably higher than the highest critical buckling stress – for specimens LC2-1, LC8 and LC12, $P_y/P_{cr.max}$ is equal to 2.38, 3.61 and 2.27, respectively.

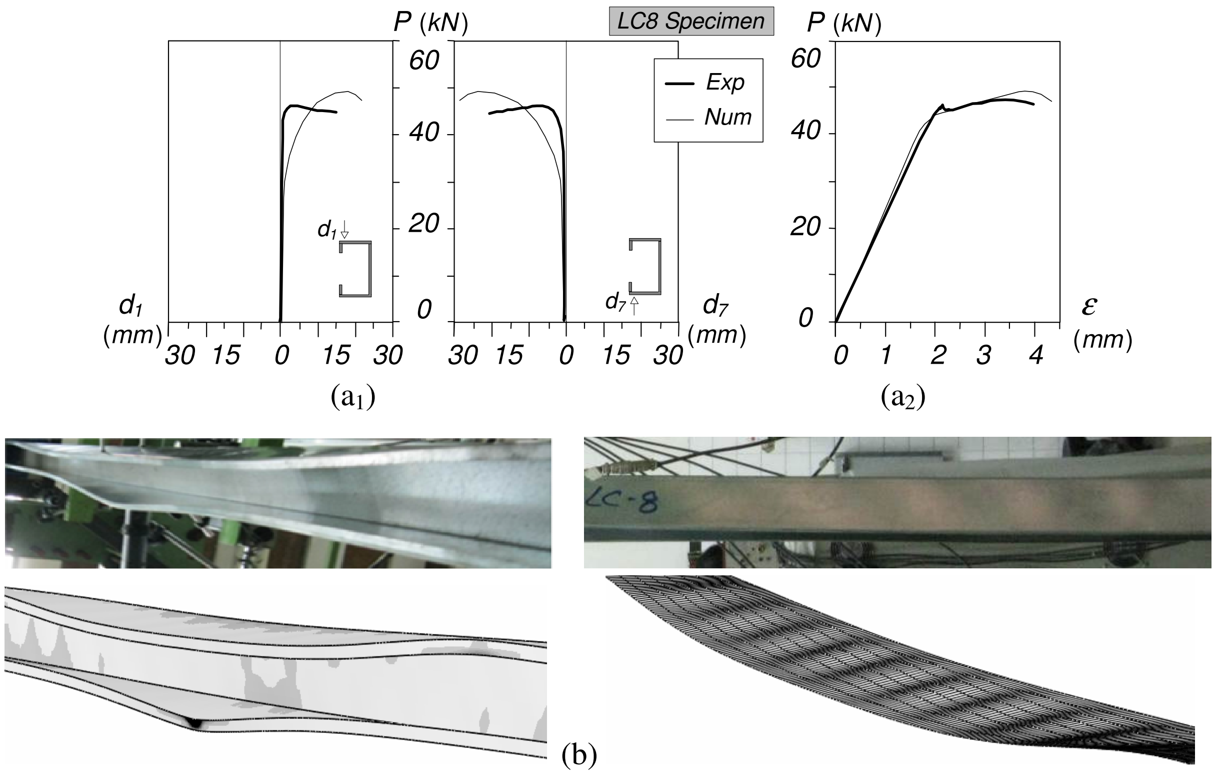

Figure 8: LC8 specimen (a) N4 numerical and experimental P vs. d_1, P vs. d_7 and P vs. ε equilibrium paths, and (b) experimental (front and back views) and numerical (N4 – front and top flange views) failure modes.

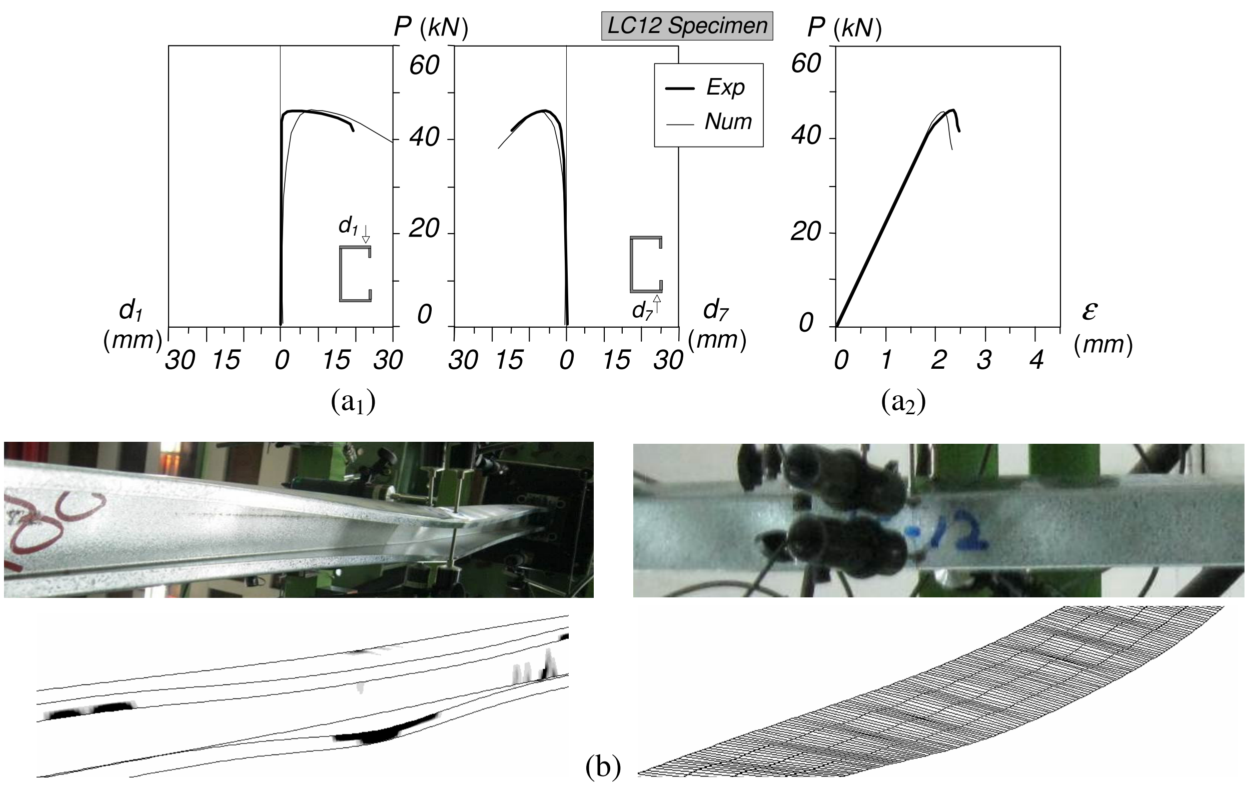

Figure 9: LC12 specimen (a) N4 numerical and experimental P vs. d_1, P vs. d_7 and P vs. ε equilibrium paths, and (b) experimental (front and back views) and numerical (N4 – front and top flange views) failure modes.

(iii) The numerical and experimental equilibrium paths P *vs.* ε correlate very well. The same is not true for the remaining equilibrium paths, namely the P *vs.* d_1 and P *vs.* d_7 curves. Indeed, even if they follow the same general trend, there are relevant differences – *e.g.*, the specimen LC2-1 P *vs.* d_1 curve obtained with N5 initial imperfections exhibits a displacement reversal near collapse that was not observed experimentally.

(iv) The major source of the discrepancies just mentioned is the insufficient (or inadequate) initial imperfection experimental data recorded – recall that all displacement were measured exclusively at the column mid-height cross-section. In order to illustrate this statement, notice that the SFEA of the LC8 specimen with initial imperfections N_1-N_5 provide failure loads overestimating the experimental value (47.46 kN) by between 3.4% to 19.5% – this means that a more accurate (realistic) initial imperfection modeling should bring the experimental and numerical results closer together.

(v) When the initial imperfections contain a global component (N_2-N_5), the failure load drops visibly, thus indicating the relevance of global deformation for the collapse of the columns analyzed[3] – *e.g.*, the specimen LC2-1 failure load decreases from 52.03 to 45.19 kN when the initial imperfections change from N_1 to N_4. Moreover, the failure loads of the columns with a FT initial imperfection component are lower than those of the columns containing a F component: *e.g.*, the specimen LC2-1 failure load increases from 45.19 to 46.62 kN when the initial imperfections change from N_4 to N_5 – 0.98% and 4.2% higher than the experimental value (44.75 kN).

(vi) The numerical equilibrium paths of the columns with N_4 initial imperfections follow fairly closely the experimental ones – in particular, note that the numerical LC8 column P *vs.* ε curve practically coincides with the experimental one up to failure. However, there are a few differences between the numerical and experimental P *vs.* d_1 and P *vs.* d_7 equilibrium paths, as the former exhibit more ductility (the numerical displacements at collapse are higher than those measured in the tests).

(vii) The three specimen failure loads are safely estimated adopting (vii_1) an elastic-perfectly plastic steel material behavior with the measured yield stress values (*i.e.*, $f_y=\sigma_{0.2}$=597 or 594 MPa, for the G550 and G500 steel grades) and (vii_2) a pure single half-wave FT initial imperfection with amplitude L/1000. Indeed, the numerical failure loads obtained read P_{Num}=43.56, 46.41 and 43.62 kN for the LC2-1, LC8 and LC12 specimens – 2.7%, 2.2% and 5.7% lower than the corresponding experimental values.

(viii) On the basis of the above comparisons, it seems fair to conclude that the SFE model employed is able to capture adequately the geometrically and materially non-linear (post-buckling) behavior and strength of CFS lipped channel columns experiencing L-D-G interaction. Therefore, this model will be used to perform parametric studies aimed at gathering additional column failure load data to cover a wide global slenderness range.

5. Ultimate Strength Data: Test Results and Numerical Predictions

In order to assess the merits (accuracy and safety) of the DSM-based design approaches that have been considered to estimate the ultimate strength of CFS fixed-ended lipped channel columns affected by L-D-G interaction, it is indispensable to assemble a large enough set of column failure loads, comprising both experimental and numerical values. Next, the experimental and numerical failure load data gathered are addressed separately.

---

[3] This agrees with the findings reported by Dinis & Camotim (2011), Dinis *et al.* (2014) and Cava *et al.* (2015), where it was concluded that, for a given (common) initial imperfection amplitude, the global (flexural-torsional) buckling mode shape is the most detrimental one, in the sense that it leads to the lowest failure load.

5.1 Experimental Failure Loads

Concerning the experimental results considered in this work, they are (i) the 17 failure loads obtained in the UHK test program, involving specimens with $1.39 \geq P_{cr.max}/P_{cr.min} \geq 1.11$ and $3.04 \geq P_y/P_{cr.max} \geq 1.43$, and (ii) additional sets of experimental failure loads collected from the literature[4]. The latter concern (i) two tests reported by Young & Rasmussen (1998) and performed at the University of Sydney, for which $P_{cr.max}/P_{cr.min}$ and $P_y/P_{cr.max}$ are equal to (2.33;0.94) and (1.47;1.46), respectively, (ii) five tests reported by Kwon *et al.* (2009) and performed at the University of Yeungnam, such that $1.56 \geq P_{cr.max}/P_{cr.min} \geq 1.17$ and $2.27 \geq P_y/P_{cr.max} \geq 1.27$, and (iii) the two test programs carried out at COPPE (Federal University of Rio de Janeiro – UFRJ) and reported by Santos *et al.* (2012, 2014a,b). While the first of these two test campaigns involved 12 specimens, all exhibiting close local, distortional and global critical buckling loads ($P_{cr.max}/P_{cr.min} \leq 1.10$) and $P_y/P_{cr.max}$ values in the 1.19-2.16 range, the second one comprised 16 specimens, all exhibiting critical local buckling (*i.e.*, $P_{cr.min}=P_{crL}$) – the intermediate critical buckling load was global for 8 columns and distortional for 6 columns (2 columns have practical identical P_{crD} and P_{crG} values). Moreover, the $P_{cr.max}/P_{cr.min}$ and $P_y/P_{cr.max}$ ratios values were in the 1.08-1.44 and 1.01-1.82 ranges, respectively. The cross-section dimensions, lengths and critical buckling loads of the 35 specimens collected from the literature are given in Table 3. In addition, their yield (f_y) and ultimate (f_{Exp}) stresses are provided in Annex A (Tables A2 to A5).

At this stage, it is worth pointing out that a subsequent revisit and close inspection of the experimental set-up, procedure and results of the first test campaign carried out at COPPE (Santos *et al.* 2012) led the authors to believe that fully fixed end support conditions had not been achieved in these tests and prompted the performance of the second test campaign[5]. This was due to the fact that, in the first test campaign, the specimen end cross-sections were deficiently welded to the rigid end plates and, therefore, full support fixity was not ensured at the most advanced loading stages (prior to collapse). This flaw was corrected in the second test campaign, in which the specimen end cross-sections were very carefully welded to the rigid end plates and, moreover, the angles between the specimen webs and rigid end plates were closely monitored during the load application process – Figs. 10(a)-(c) show the test set-up employed in the second experimental study carried out at COPPE (Santos *et al.* 2014a), including detailed views of the fixed end supports (and of the measurement made to monitor their "quality")[6]. Although there are no visible differences in the collapse modes observed in the specimens tested in the two COPPE experimental studies, as can be attested by looking at Figs. 11(a)-(f), the ultimate strength values (f_{Exp}) are generally considerably larger, which can be confirmed by comparing the results presented by Dinis *et al.* (2015). This is due to the absence of fully fixed end supports in the first test campaign. Indeed, it is well known that the presence of a finite rotational restraint/spring (even if very large/stiff) entails non-

[4] Some experimental failure loads were taken from publications reporting research work that either (i) was not specifically intended to investigate the triple coupling phenomenon under consideration in this paper or (ii) did not involve exclusively lipped channel specimens. The only failure loads considered here concern lipped channel specimens for which either (i) local, distortional and global (flexural-torsional) deformations were visually observed at failure or (ii) exhibiting close local, distortional and global critical buckling loads.

[5] Note that very detailed information is available about the COPPE and UHK tests, since the authors were involved in their performance. On the other hand, the information and results concerning the tests carried out at the University of Sydney and the University of Yeungnam were taken from the literature.

[6] Although no deviations from the normality between the webs and end plates were detected, it is still possible that these plates experienced small flexural rotations, due to the bottom support arrangement shown in Fig. 10(a)-(c) (several rigid plates loosely stacked on top of a rigid plate "indirectly bolted" to the test machine lower cross-beam – the rigid plate number varies with the specimen length). In any case, the flexural rotations are always much smaller than those due to the welding deficiencies detected in the first test campaign.

Table 3: Tested specimen geometries and critical (L, D, G) buckling loads and ratios

	Specimen	b_w (mm)	b_f (mm)	b_s (mm)	t (mm)	L (mm)	P_{crL} (kN)	P_{crD} (kN)	P_{crG} (kN)	$\frac{P_{cr.int}}{P_{cr.min}}$	$\frac{P_{cr.max}}{P_{cr.min}}$
Young & Rasmussen (1998)	L48F1500	96.5	48.9	12.6	1.46	1501	78.5	109.6	182.7	1.40	2.33
	L48F2000	97.5	49.3	11.9	1.47	2001	80.5	103.4	118.6	1.28	1.47
Kwon *et al.* (2009)	A-6-1-1200	40.0	40.0	10.0	0.60	1200	15.0	22.9	21.3	1.42	1.53
	A-8-1-1200	50.0	40.0	10.0	0.80	1200	28.6	37.9	41.2	1.32	1.44
	A-8-2-800	40.0	40.0	10.0	0.80	800	34.9	43.5	54.5	1.25	1.56
	A-8-2-1000	40.0	40.0	10.0	0.80	1000	34.9	40.9	39.8	1.14	1.17
	A-8-2-1200	40.0	40.0	10.0	0.80	1200	34.9	38.3	29.5	1.19	1.30
Santos *et al.* (2012)	C1	82.7	77.4	12.0	1.06	2850	43.8	42.9	44.1	1.03	1.03
	C2	82.0	77.8	11.9	1.06	2850	43.8	42.9	44.1	1.03	1.03
	C3	82.0	77.5	11.9	1.07	2850	43.8	42.9	44.1	1.03	1.03
	C4	76.3	64.4	10.8	1.07	2352	48.8	47.5	48.6	1.02	1.03
	C5	75.7	64.4	10.9	1.07	2349	48.8	47.5	48.6	1.02	1.03
	C6	75.7	64.4	10.9	1.07	2349	48.8	47.5	48.6	1.02	1.03
	C7	72.4	59.3	11.0	1.07	2099	51.9	51.8	51.9	1.00	1.00
	C8	72.4	59.1	11.1	1.06	2099	51.9	51.8	51.9	1.00	1.00
	C9	62.5	54.4	10.9	1.08	1652	60.1	58.8	59.5	1.01	1.02
	C10	62.8	54.2	11.3	1.08	1650	60.1	58.8	59.5	1.01	1.02
	C21	76.9	60.9	10.9	1.09	2350	48.8	48.0	49.9	1.04	1.04
	C22	77.3	60.7	11.1	1.08	2350	48.8	48.0	49.9	1.04	1.04
Santos *et al.* (2014a)	CP2	79.4	66.1	11.8	1.08	2600	44.0	48.1	46.2	1.05	1.09
	CP4	79.3	66.0	11.8	1.08	2550	44.0	48.3	47.6	1.08	1.10
	CP6	78.9	66.0	11.8	1.09	2500	45.5	49.3	49.3	1.08	1.08
	CP8	79.6	65.8	12.0	1.09	2350	45.1	50.7	55.5	1.12	1.23
	CP10	78.4	66.5	11.9	1.09	2200	45.9	50.7	59.3	1.11	1.29
	CP12	79.8	65.7	11.8	1.10	2150	46.2	51.9	63.3	1.13	1.37
	CP14	75.3	61.5	11.7	1.09	2350	47.8	52.5	49.2	1.03	1.10
	CP16	74.7	61.0	11.9	1.09	2300	48.4	53.9	50.5	1.04	1.11
	CP18	75.3	61.1	11.8	1.07	2250	45.3	51.5	51.7	1.14	1.14
	CP20	75.2	61.3	11.8	1.08	2100	46.6	53.3	57.6	1.14	1.24
	CP22	66.8	56.2	11.8	1.08	1900	53.3	58.8	55.3	1.04	1.10
	CP24	66.7	56.0	11.7	1.07	1850	51.9	57.6	56.6	1.09	1.11
	CP26	66.6	56.0	11.8	1.07	1800	52.1	58.0	59.1	1.12	1.14
	CP28	66.8	55.9	11.8	1.08	1650	53.3	59.7	67.9	1.12	1.27
	CP30	66.8	56.0	11.7	1.09	1550	54.8	61.1	73.6	1.12	1.34
	CP32	66.5	56.1	11.7	1.08	1500	53.6	60.7	74.6	1.13	1.39

negligible drops in the column global (mostly) and distortional critical buckling loads (the influence of the boundary conditions on the local critical buckling is much smaller, due to the large number of half-waves exhibited by the corresponding buckling mode). Since the column collapse is chiefly governed by global buckling, a drop in the associated critical load automatically causes an ultimate strength decrease.

In spite of what was mentioned in the previous paragraph, the results of the COPPE first test campaign were also included in the column failure load data considered in this work, thus bringing the total number of experimental failure loads to 52. Nevertheless, it is to be expected that the 12 experimental failure loads obtained from those tests will lie below the remaining ones (experimental and numerical), which concern really fixed-ended columns.

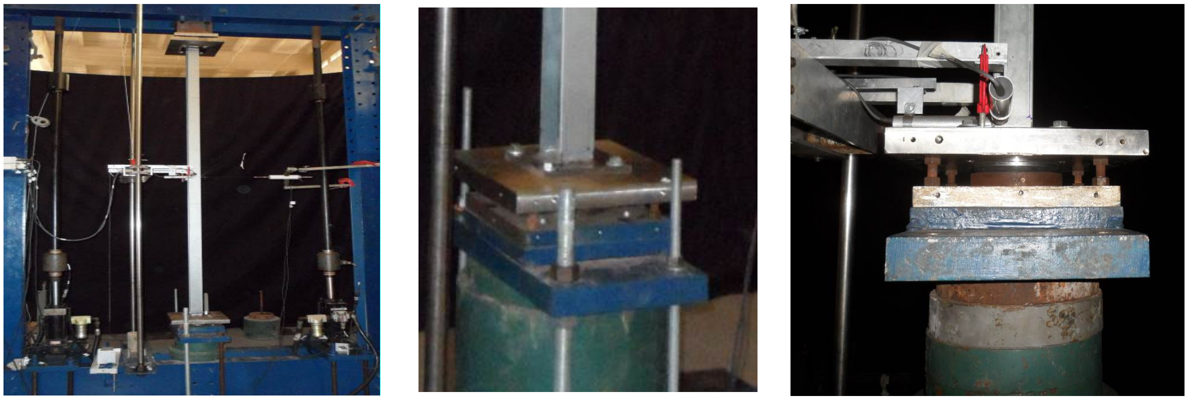

(a) (b) (c)

Figure 10: Experimental set-up of the COPPE second test campaign: (a) general view, (b) fixed end support and (c) monitoring of the angle between the specimen web and end plate (Santos *et al*. 2014a)

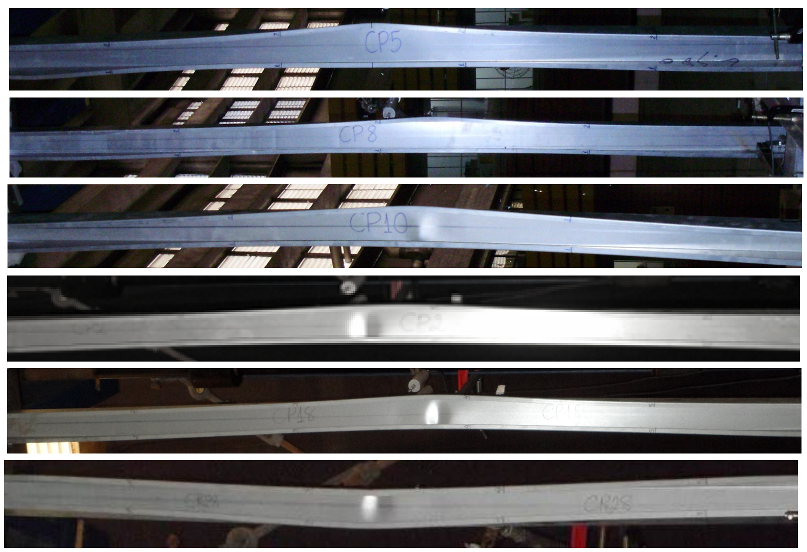

(a)
(b)
(c)
(d)
(e)
(f)

Figure 11: Deformed configurations at the onset of collapse ($P \approx P_{exp}$) of the COPPE tests: (a)-(c) first test campaign (specimens C5, C8, C10) (Santos *et al*. 2012) and (d)-(f) second test campaign (specimens CP2, CP18, CP28) (Santos *et al*. 2014a)

Finally, a few last words to mention a distinctive feature between the failure modes of the specimens tested at the UHK and at COPPE (Santos *et al.* 2012,2014a): while local deformations are clearly visible in the former (see Figs. 5(a)-(b), 7(b), 8(b) and 9(b)), they are barely perceptible in the latter (see Figs. 11(a)-(f)). This difference is due to a combination of specimen geometrical and material characteristics, namely (i) the relative values of the local, distortional and global critical buckling loads, (ii) the initial geometrical imperfection configuration and (iii) the yield stress. In order to provide an illustration of the above assertion, Figs. 12(a)-(b) show the numerically obtained collapse modes of columns with (i) b_w=66.8 mm, b_f=55.9 mm, b_s=11.8 mm, t=1.08 mm, L=1650 mm (L column – identical to specimen C28 tested by Santos *et al.* (2014a): $f_{crL}=f_{cr.min}$=244.3 MPa, $f_{crD}=1.12f_{cr.min}$, $f_{crG}=f_{cr.max}=1.27f_{cr.min}$, $f_y=1.20f_{cr.max}$), (ii) b_w=85.0 mm, b_f=75.0 mm, b_s=12.0 mm, t=1.4 mm, L=2700 mm (G column – $f_{crG}=f_{cr.min}$=191.9 MPa, $f_{crD}=1.06f_{cr.min}$, $f_{crL}=f_{cr.max}=1.26f_{cr.min}$, $f_y=1.24f_{cr.max}$), both containing pure global initial imperfections with amplitude L/1000. Note that the numerical failure modes obtained either (i) combine local, distortional and global deformations (L column) or (ii) exhibit a combination of global (mostly) and distortional deformations (G column).

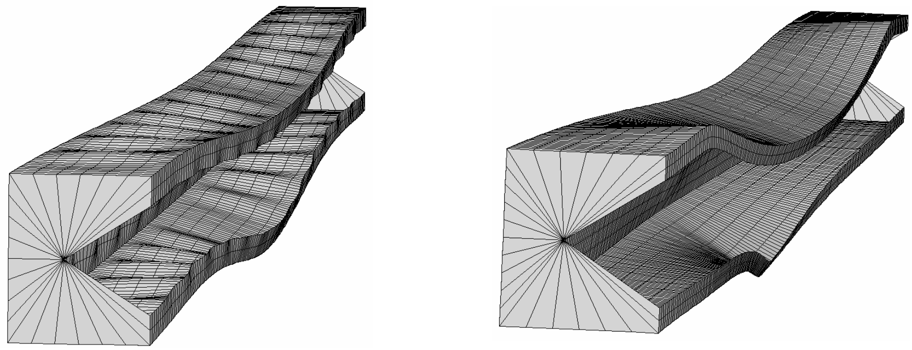

(a) (b)

Figure 12: Numerical failure modes obtained for columns with critical (a) local and (b) global critical buckling loads and pure global initial imperfections (the former is amplified 8 times)

5.2 Numerical Failure Loads

The numerical failure loads considered in this work correspond to 893 columns either analyzed in previous works or obtained in the course of the present investigation. Concerning the former, there are (i) 134 failure loads reported by Dinis *et al.* (2012), for columns with $1.00 \leq P_{cr.max}/P_{cr.min} \leq 1.10$ and $0.53 \leq P_y/P_{cr.max} \leq 6.24$, and (ii) 391 failure loads obtained recently by Cava *et al.* (2015), for columns with $1.27 \geq P_{cr.max}/P_{cr.min} \geq 1.02$ and $\lambda_G=(f_y/f_{crG})^{0.5}$ varying from 0.5 to 2.5 in 0.5 intervals. The failure loads of the remaining 368 columns, obtained in this work, concern columns exhibiting (i) the geometries of the specimens tested at UHK (LC_N columns, such that $1.39 \geq P_{cr.max}/P_{cr.min} \geq 1.11$), and (ii) 50 geometries selected from those identified by Cava (2015) (LP_N columns, such that $1.27 \geq P_{cr.max}/P_{cr.min} \geq 1.04$). The yield stress values f_y were chosen to enable covering a wide global slenderness (λ_G) range and having a fairly even "horizontal (along the λ_G axis) distribution" of the f_U/f_y values in the f_U/f_y vs. λ_G plots[7]. In order to achieve these goals, the columns analyzed have yield stresses (i) f_y=300, 500, 700, 900 MPa (LC_N columns with $5.41 \geq P_y/P_{cr.max} \geq 0.81$) and (ii) f_y=300, 450, 600, 750, 900, 1200 MPa (LP_N columns with $6.87 \geq P_y/P_{cr.max} \geq 0.63$) – the authors acknowledge that some of these f_y values are unrealistically high (they were considered for the sake of completion). Following the conclusions drawn from the comparison between experimental and SFEA results, reported earlier, it was decided (i) to model the steel material behavior as elastic-perfectly plastic (E=210 GPa, ν=0.3), (ii) to disregard both residual stresses and rounded corner effects (they usually cancel each other), and (iii) to determine failure loads of columns containing (critical-mode) flexural-torsional initial geometrical imperfections[8] with amplitude L/1000, value in line with the measurements reported for the specimens tested at UHK. The ultimate stresses (f_{Num}) obtained for the LC_N and LP_N columns are given, in tabular form, in Annex B (Tables B1 and B2, respectively). In the latter case, the LP_N column cross-section dimensions, lengths and critical buckling stresses are also shown. Figs. 13(a)-(b), concerning columns with b_w=75 mm, b_f=65 mm, b_s=11 mm, t=1.1 mm, L=2350 mm and various yield stresses, illustrate the equilibrium paths that it was necessary to determine in order to obtain the numerical failure load data presented in Annex B.

[7] Indeed, note that, for instance, Cava *et al.* (2015) considered the same five λ_G values for all the columns analyzed, which led to f_U/f_y values located along five vertical lines – the failure loads added in this work (for those same columns), make it possible to have a reasonably even distribution along the λ_G axis.

[8] This initial geometrical imperfection shape was found to be the most detrimental, in the sense that it leads to the lowest column strength and failure load (Dinis & Camotim 2011, Dinis *et al.* 2011, 2012, Cava *et al.* 2015).

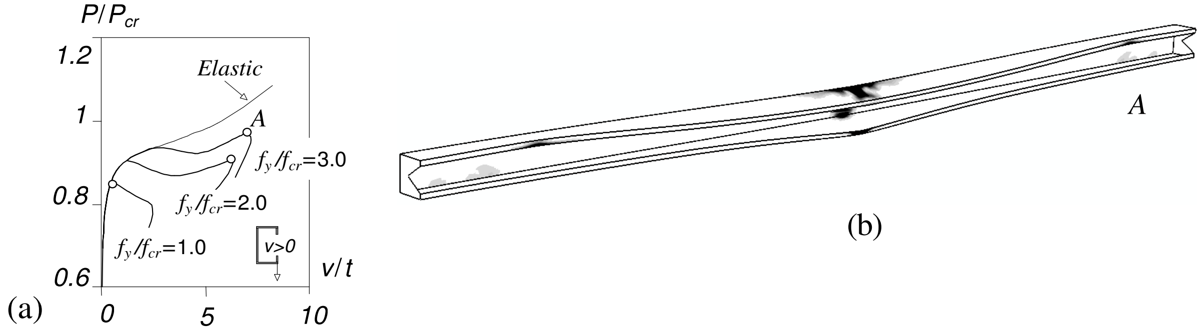

Figure 13: Columns with b_w=75 mm, b_f=65 mm, b_s=11 mm, t=1.1 mm, L=2350 mm: (a) elastic-plastic P/P_{cr} *vs.* v/t equilibrium paths, for f_y/f_{cr}=1.0; 2.0; 3.0; ∞; and (b) deformed configuration and plastic strains at collapse, for f_y/f_{cr}=3.0

6. DSM Design Considerations

The currently codified DSM column design curves (*e.g.*, Schafer 2008) provide nominal strengths against local, distortional, global and local-global interactive failures (f_{NL}, f_{ND}, f_{NG} and f_{NLG}) − in the last case, f_y is replaced by f_{NG} in the f_{NL} expressions. However, no similarly well established and consensual strength curves are yet available for interactive failures involving distortional buckling. Following the procedure adopted to handle local-global interactive failures, it is possible to develop DSM-based design procedures intended to estimate the ultimate strength of columns failing in local-distortional or distortional-global interactive modes, by replacing (i) f_y with f_{ND} in the f_{NL} equations (f_{NLD} approach) or (ii) f_y with f_{NG} in the f_{ND} equations (f_{NDG} approach), as first suggested by Schafer (2002). A modified version of the first procedure was proposed by Silvestre *et al.* (2012), in the context of lipped channel columns undergoing local-distortional interaction, and later extended to hat-section, zed-section and rack-section columns under the same circumstances (Dinis & Camotim 2015) − this design approach was shown to be rather efficient (safe and accurate) and is expected to be codified in the not too distant future. As for the second procedure, it was employed by Yap & Hancock (2011), in the context of web-stiffened lipped channel columns experiencing distortional-global interaction. Moreover, these authors carried the same reasoning one step further and argued that it may be possible to predict the failure loads of cold-formed steel columns affected by triple (L-D-G) interaction using f_{NLDG} values, obtained from the f_{NL} expressions through the replacement of f_y with f_{NDG}. Therefore, the available column nominal strengths against interactive failures involving global buckling are given by:

$$f_{NLG}=\begin{cases} f_{NG} & \text{if} \quad \lambda_{LG}\le 0.776 \\ f_{NG}\left(\dfrac{f_{CRL}}{f_{NG}}\right)^{0.4}\left[1-0.15\left(\dfrac{f_{CRL}}{f_{NG}}\right)^{0.4}\right] & \text{if} \quad \lambda_{LG}>0.776 \end{cases} \quad \text{where} \quad \lambda_{LG}=\sqrt{\frac{f_{NG}}{f_{CRL}}} \quad , \quad (1)$$

$$f_{NDG}=\begin{cases} f_{NG} & \text{if} \quad \lambda_{DG}\le 0.561 \\ f_{NG}\left(\dfrac{f_{CRD}}{f_{NG}}\right)^{0.6}\left[1-0.25\left(\dfrac{f_{CRD}}{f_{NG}}\right)^{0.6}\right] & \text{if} \quad \lambda_{DG}>0.561 \end{cases} \quad \text{where} \quad \lambda_{DG}=\sqrt{\frac{f_{NG}}{f_{CRD}}} \quad , \quad (2)$$

$$f_{NLDG}=\begin{cases} f_{NDG} & \text{if} \quad \lambda_{LDG}\le 0.776 \\ f_{NDG}\left(\dfrac{f_{CRL}}{f_{NDG}}\right)^{0.4}\left[1-0.15\left(\dfrac{f_{CRL}}{f_{NDG}}\right)^{0.4}\right] & \text{if} \quad \lambda_{LDG}>0.776 \end{cases} \quad \text{where} \quad \lambda_{LDG}=\sqrt{\frac{f_{NDG}}{f_{CRL}}} \quad . \quad (3)$$

Fig. 14(a) compares the three above DSM strength curves (LG, DG and LDG), plotted against the global slenderness λ_G[9], with the failure stress ratios f_U/f_y concerning the 52 fixed-ended lipped channel columns experimentally tested at (i) the UHK (f_y is the measured yield stress), identified by 17 white circles (LC_E columns), and (ii) the University of Sydney (Young & Rasmussen 1998), identified by 2 white squares, (iii) the University of Yeungnam (Kwon *et al.* 2009), identified by 5 white triangles, and (iv) at the Federal University of Rio de Janeiro (COPPE), identified by 12 black circles (first test campaign – Santos *et al.* 2012) and 16 grey circles (second test campaign – Santos *et al.* 2014a). On the other hand, Fig. 14(b) displays similar results concerning the 893 fixed-ended lipped channel columns numerically analyzed (i) by Dinis *et al.* (2012), identified by 134 white triangles, (ii) by Cava *et al.* (2015), identified by 391 white rectangles, and (iii) in the course of this study, identified by 68 grey circles (LC_N columns) and 300 grey triangles (LP_N columns). Finally, Figs. 15(a)-(c) plot, for the whole set of columns, the ultimate-to-predicted strength ratios f_U/f_{NLG}, f_U/f_{NDG}, f_U/f_{NLDG} against λ_G – the corresponding mean, standard deviation, maximum and minimum values are given in Table 4. The observation of these results makes it possible to conclude that:

(i) As anticipated, the experimental ultimate strengths obtained from the first test campaign carried out by Santos *et al.* (2012) fall below all the remaining ones, including those concerning the second test campaign carried out at COPPE. It should also be noted that the experimental ultimate strengths reported by Kwon *et al.* (2009) are also generally lower than those reported by the other authors, which may be again due to the inability to ensure fully fixed ended support conditions. In this case, such conditions were achieved by means of the arrangement depicted in Fig. 16[10], which involves embedding the specimen end cross-section in polyester resin capping systems – if such arrangements are not capable of ensuring fully fixed-ended columns at high load levels (as the authors believe[11]), it seems logical to expect lower experimental failure loads.

(ii) With the exception of the lower ultimate strength values addressed in the previous item, it is fair to say that the numerical and experimental f_U/f_y values correlate extremely well – moreover, all these values are nicely aligned along a "Winter-type" curve with small vertical dispersion.

(iii) In spite of the different critical load ratios considered, the cloud of numerical f_U/f_y values obtained for the LC_N and LP_N columns is practically undistinguishable from those reported by Dinis *et al.* (2012) and Cava *et al.* (2015). It is worth recalling that (iii_1) $1.39 \geq P_{cr.max}/P_{cr.min} \geq 1.11$ (LC_N columns), (iii_2) $1.27 \geq P_{cr.max}/P_{cr.min} \geq 1.04$ (LP_N columns), (iii_3) $1.10 \geq P_{cr.max}/P_{cr.min} \geq 1.00$ (columns in Dinis *et al.* 2012) and (iii_4) $1.27 \geq P_{cr.max}/P_{cr.min} \geq 1.02$ (columns in Cava *et al.* 2015) – moreover, the sequence and closeness of the local, distortional and global critical buckling loads are so diverse that it may be argued that they have been selected (nearly) randomly. In particular, several columns analyzed had either (iii_1) all critical buckling loads very close or (iii_2) local critical buckling loads well below their distortional and global counterparts, thus implying a substantial post-critical strength reserve – two situations corresponding to a high ultimate strength erosion stemming from triple interaction effects.

(iv) The f_{NLG} design approach provides mostly safe predictions of the column experimental and numerical failure loads and, with the exception of the experimental values obtained from the COPPE

[9] Obviously, the joint representation of the three design curves is made under the assumption that $\lambda_L \approx \lambda_D \approx \lambda_G$, which is clearly a fairly crude approximation is some cases. A more accurate account would require a different plot for each design curve, thus making their comparison much less clear.

[10] The specimen shown in Fig. 16 has a web-stiffened lipped channel cross-section. The experimental investigation reported by Kwon *et al.* (2009) involved columns with several cross-section shapes – only the results concerning tests on column specimens with "plain" lipped channel cross-sections (affected by L-D-G interaction) were retained in this work (5 tests).

[11] A similar conclusion was reached by Martins *et al.* (2015a) for the tests involving lipped channel columns undergoing local-distortional (L-D) interaction.

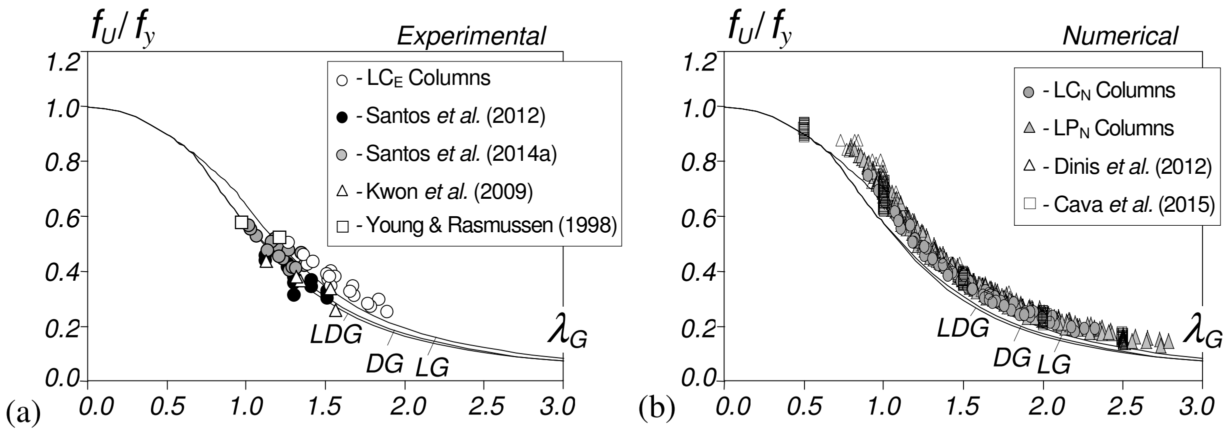

Figure 14: DSM design curves against interactive failures and plots of f_U/f_y against λ_G for the column analyzed (a) experimentally and (b) numerically

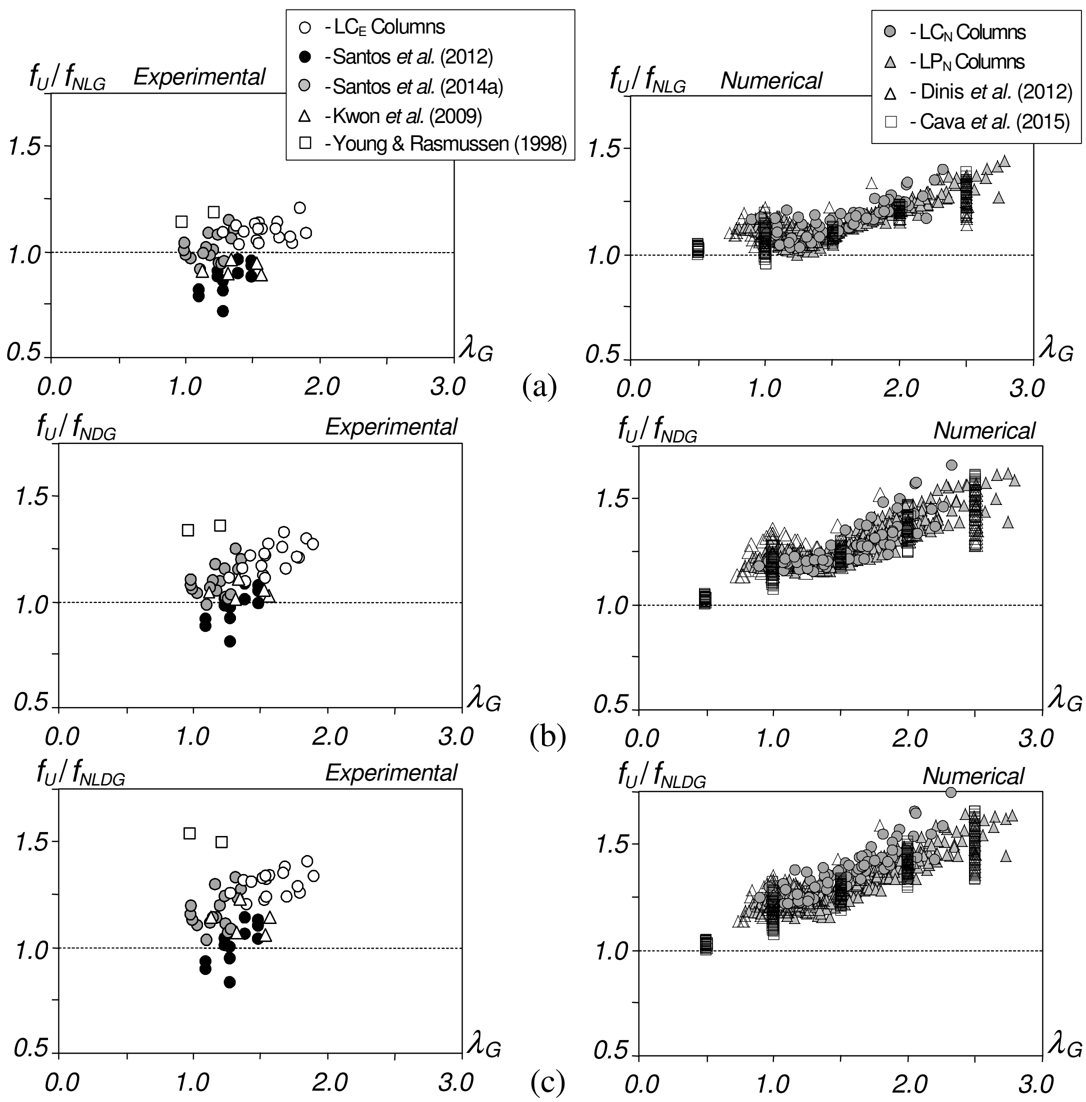

Figure 15: Plots of the ultimate-to-predicted strength ratios (a) f_U/f_{NLG}, (b) f_U/f_{NDG} and (c) f_U/f_{NLDG} against the global slenderness λ_G

Table 4: Means, standard deviations, maximum and minimum values of the ultimate-to-predicted strength ratios provided by the different DSM design approaches.

Failure-to-predicted strength ratios			f_U/f_{NLG}	f_U/f_{NDG}	f_U/f_{NLDG}
Experimental	LC_E especimens	Mean	1.21	1.34	1.46
		S. Dev.	0.05	0.08	0.07
		Min	1.14	1.21	1.34
		Max	1.35	1.49	1.58
	Santos *et al* (2012)	Mean	0.86	0.97	1.01
		S. Dev.	0.07	0.08	0.09
		Min	0.71	0.81	0.83
		Max	0.96	1.08	1.14
	Santos *et al* (2014a)	Mean	1.00	1.09	1.16
		S. Dev.	0.07	0.08	0.09
		Min	0.91	0.98	1.03
		Max	1.14	1.25	1.33
	Kwon *et al* (2009)	Mean	0.92	1.05	1.14
		S. Dev.	0.03	0.04	0.07
		Min	0.89	1.02	1.07
		Max	0.97	1.11	1.24
	Young & Rasmussen (1998)	Mean	1.16	1.35	1.52
		S. Dev.	0.03	0.02	0.03
		Min	1.14	1.34	1.50
		Max	1.19	1.36	1.54
	All tests	Mean	1.04	1.15	1.24
		S. Dev.	0.15	0.17	0.20
		Min	1.35	1.50	1.59
		Max	0.71	0.81	0.83
Numerical	LC_N columns	Mean	1.16	1.28	1.38
		S. Dev.	0.08	0.11	0.11
		Min	1.03	1.15	1.21
		Max	1.40	1.65	1.74
	LP_N columns	Mean	1.15	1.29	1.33
		S. Dev.	0.08	0.10	0.11
		Min	1.00	1.16	1.16
		Max	1.44	1.63	1.65
	Dinis *et al* (2012)	Mean	1.13	1.28	1.31
		S. Dev.	0.07	0.10	0.11
		Min	1.01	1.14	1.14
		Max	1.37	1.54	1.61
	Cava *et al* (2015)	Mean	1.16	1.29	1.31
		S. Dev.	0.13	0.18	0.20
		Min	0.95	1.00	1.00
		Max	1.45	1.73	1.77
	All simulations	Mean	1.15	1.29	1.32
		S. Dev.	0.10	0.15	0.16
		Min	1.45	1.73	1.77
		Max	0.95	1.00	1.00

first test campaign, the relatively few overestimations are never more than mildly pronounced. As for the f_{NDG} and f_{NLDG} values, they underestimate all but the experimental f_U values of the COPPE first tests series – obviously, the f_{NLG} values are the smallest ones. A large number of underestimations are clearly excessive, particularly those concerning the numerical f_U values of the most slender columns.

(v) The indicators of the f_U/f_{NLG} ratio, given in Table 4, show that only (v_1) values associated with the COPPE first test campaign are below 0.89 and (v_2) the mean values concerning the experimental results reported by Santos *et al.* (2012) and Kwon *et al.* (2009) fall below 1.0 (0.86 and 0.92, respectively). Moreover, the mean values and standard deviation of the various sets of numerical f_U/f_{NLG} values range from 1.13 to 1.16 and from 0.07 to 0.13, respectively.

(vi) The currently codified DSM design/strength curve against local-global interactive failures predicts the whole set of experimental and numerical CFS lipped channel column failure loads considered in this work quite well. Indeed, the f_U/f_{NLG} mean values and standard deviations are equal to 1.04/0.15 (experimental), 1.15/0.10 (numerical) and 1.13/0.10 (experimental and numerical) – if the results obtained from the COPPE first test campaign are excluded, the first and third pairs of indicators improve to 1.14/0.091 and 1.13/0.093, respectively.

Figure 16: Arrangement to ensure fixed end supports in the tests reported performed at the University of Yeungnam (Kwon *et al.* 2009): end cross-section embedded in a polyester resin capping

6.1 Load and Resistance Factor Design (LRFD)

The evaluation of the LRFD (Load and Resistance Factor Design) resistance factor ϕ associated with the use of the currently codified DSM design/strength curve against local-global interactive failures to predict the ultimate strength of the CFS lipped channel columns undergoing L-D-G interaction is addressed next. According to the North American cold-formed steel specification (AISI 2012), ϕ can be calculated by means of the formula given in section F.1.1 of chapter F, which reads

$$\phi = C_\phi (M_m F_m P_m)\, e^{-\beta_0 \sqrt{V_M^2 + V_F^2 + C_P V_P^2 + V_Q^2}} \qquad \text{with} \qquad C_P = \left(1 + \frac{1}{n}\right)\frac{m}{m-2} \quad , \tag{4}$$

where (i) C_ϕ is a calibration coefficient (C_ϕ=1.52 for LRFD), (ii) M_m=1.10 and F_m=1.00 are the mean values of the material and fabrication factors, respectively, (iii) β_0 is the target reliability index (β_0=2.5 for structural members in LRFD), (iv) V_M=0.10, V_F=0.05 and V_Q=0.21 are the coefficients of variation of the material factor, fabrication factor and load effect, respectively, and (v) C_P is a correction factor depending on the numbers of tests (n) and degrees of freedom (m=n-1). In order to evaluate ϕ for the case under consideration it is necessary to calculate P_m and V_P, which are the mean and standard deviation of the "exact"-to-predicted strength ratios f_U/f_{NLG} – the "exact" f_U values are either experimental, numerical or experimental and numerical.

Table 5 shows the n, C_P, P_m, V_P and ϕ values obtained for the column ultimate strength predictions provided by the f_{NLG} procedure applied to the experimental (EXP), numerical (NUM) and total (EXP+NUM) failure load data – also included are values concerning the exclusion of the ultimate strengths obtained from the COPPE first test campaign (EXP*). It is observed that:

(i) When all the failure load data are considered, the resistance factors values obtained are (i_1) ϕ=0.85 (experimental), (i_2) ϕ=1.00 (numerical) and (i_3) ϕ=0.99 (experimental and numerical) – obviously, in view of the disparity between the numbers of experimental and numerical ultimate strength values available, the last two resistance factors are practically identical. These values are either identical or higher (better) than the one recommended by the North American specification for cold-formed steel compression members (ϕ=0.85).

(ii) When the COPPE first test campaign is excluded, the ϕ values become ϕ=0.92 (experimental) and ϕ=1.00 (experimental and numerical).

(iii) It seems fair to conclude the currently codified DSM design curve against local-global interactive failure provides excellent predictions of the failure load of CFS lipped channel columns undergoing local-distortional-global interaction.

Table 5: DSM f_{NLG} procedure: LRFD resistance factors ϕ calculated according to AISI (2012)

	DSM f_{NLG} procedure				
	EXP	EXP*	NUM	EXP+NUM	EXP*+NUM
n	52	40	893	945	933
C_P	1.061	1.080	1.003	1.003	1.003
P_m	1.041	1.094	1.146	1.131	1.134
V_P	0.155	0.131	0.097	0.098	0.093
ϕ	0.85	0.92	1.00	0.99	1.00

7. Conclusion

An experimental and numerical investigation on the post-buckling behavior, ultimate strength and design of cold-formed steel fixed-ended lipped channel columns affected by various levels of local-distortional-global mode interaction was reported – the three critical buckling loads involved may be more or less close and in any given sequence. After briefly addressing the selection of the column specimen geometries and the possible types of interaction, the paper presented the most relevant results of an experimental campaign carried out at The University of Hong Kong (UHK) comprising 17 specimens – they consisted of initial imperfections, equilibrium paths and failure loads and modes, which provided clear evidence of the occurrence of the above coupling phenomenon. Then, numerical simulations of three experimental tests carried out at UHK were presented and discussed, which made it possible to improve and calibrate the ABAQUS shell finite element model developed. In particular, the performance of an imperfection-sensitivity study led to the identification of the most detrimental initial imperfections, which was subsequently used in a parametric study, intended to gather additional column failure load data – the columns analyzed had either (i) the geometries of the specimens tested at UHK and several yield stresses, selected to enable covering a wide global slenderness range, or (ii) the cross-section shapes identified by Cava *et al.* (2015), selecting various yield stresses to cover continuously the slenderness range under consideration. Then, the (i) 17 experimental failure loads obtained at UHK, (ii) 35 other experimental failure loads collected from literature, (iii) 368 numerical failure loads determined in this study and (iv) 525 numerical failure loads determined earlier by the authors were used to assess the merits of a few available design approaches, based on the Direct Strength Method (DSM), which have been tentatively put forward by several authors to capture the ultimate strength erosion stemming from interaction phenomena involving global buckling, namely the so-called NLG, NDG and NLDG approaches – a total of 52 experimental and 893 numerical lipped channel fixed-ended column failure loads were considered to perform this task.

The main achievements of the experimental investigation were (i) providing clear experimental evidence of the occurrence of L-D-G triple interaction, and (ii) quantifying its influence on the column deformed configuration evolution, including the failure mode, and ultimate strength erosion. Moreover, another important finding of this work was the fact that the local deformations were clearly observed, which did not occur in similar tests carried out by Santos *et al.* (2012, 2014a) – indeed, those authors reported that local deformations have virtually no influence on the post-buckling behavior and load-carrying capacity of CFS lipped channel columns experiencing "true L-D-G interaction".

Then, the paper (i) provided clear numerical evidence of the occurrence of L-D-G (triple) interaction, thus confirming the experimental findings, and (ii) showed that efficient (accurate and mostly safe) failure load estimates of lipped channel columns experiencing L-D-G interaction are yielded by the currently codified DSM against local-global interactive failures (NLG approach) – in other words, there is no need of an additional DSM design curve to handle adequately lipped channel columns affected by the triple coupling phenomenon under consideration. As for the remaining two DSM-based design approaches (NDG and NLDG), they were shown to provide excessively conservative/safe ultimate strength predictions, particularly in the moderate-to-high global slenderness range. Moreover, it was shown that the LRFD resistance factors obtained with the DSM NLG design approach, for the experimental and/or numerical "exact" failure loads, are perfectly in line with the value currently prescribed in AISI (2012) for member design (ϕ=0.85) – this means that the currently codified NLG design curve can be readily proposed to predict failure loads of lipped channel columns undergoing L-D-G interaction.

The next step of this ongoing research effort is to assess whether the findings reported in this paper can be extended to cold-formed steel columns having other cross-section shapes (*e.g.*, hat, zed or rack-sections) affected by L-D-G interaction. If this is the case, it will be possible to reach the general conclusion that the currently codified NLG design curve is able to handle CFS columns failing in L-D-G interactive modes.

References

American Iron and Steel Institute (AISI) (2012). North American Specification (NAS) for the Design of Cold-Formed Steel Structural Members (AISI-S100-12), Washington DC.

Bebiano R, Silvestre N, Camotim D (2008a). "GBTul – A code for the buckling analysis of cold-formed steel members", *Proceedings of 19th International Specialty Conference on Recent Research and Developments in Cold-Formed Steel Design and Construction* (St. Louis, 14-15/10), R. LaBoube, W.-W. Yu (eds.), 61-79.

Bebiano R, Silvestre N, Camotim D (2008b). GBTul 1.0b – *Code for Buckling and Vibration Analysis of Thin-Walled Members*, http://www.civil.ist.utl.pt/gbt.

Cava D (2015). *Cold-Formed Steel Lipped Channels Undergoing L/D/G Mode Interaction: Numerical Investigation and DSM Assessment*, M.A.Sc. Thesis, University of Calabria (Italy).

Cava D, Camotim D, Dinis PB, Madeo A (2015). "Numerical investigation and direct strength design of cold-formed steel lipped channel columns experiencing local-distortional-global interaction", *submitted for publication*.

Dinis PB, Camotim D (2011). "Local/distortional/global mode interaction in simply supported cold-formed steel lipped channel columns", *International Journal of Structural Stability and Dynamics*, **11**(5), 877-902.

Dinis PB, Camotim D (2015). “Cold-formed steel columns undergoing local-distortional coupling: behaviour and direct strength prediction against interactive failure”, *Computers & Structures*, **147**(January), 181-208.

Dinis PB, Camotim D, Silvestre N (2007). “FEM-based analysis of the local-plate/distortional mode interaction in cold-formed steel lipped channel columns”, *Computers & Structures*, **85**(19-20), 1461-1474.

Dinis PB, Camotim D, Batista EM, Santos ES (2011). “Local/distortional/global mode coupling in fixed lipped channel columns: behaviour and strength”, *Advanced Steel Construction - an International Journal*, **7**(4), 113-130.

Dinis PB, Batista EM, Camotim D, Santos ES (2012). “Local-distortional-global interaction in lipped channel columns: experimental results, numerical simulations and design considerations”, *Thin-Walled Structures*, **61**(December), 2-13.

Dinis PB, Young B, Camotim D (2014). “L-D-G interaction in CFS lipped channel columns: experimental results, numerical simulations and design considerations”, *Proceedings of 7th European Conference on Steel and Composite Structures* (Eurosteel 2014 – Naples, 10-12/9), 419-420. (full paper in USB Key Drive Proceedings – Paper 583).

Dinis PB, Camotim D, Young B (2015). “L-D-G Interaction in CFS lipped channel columns – part II: numerical simulations and design considerations”, *Proceedings of 15th International Conference on Civil, Structural and Environmental Engineering Computing* (CC 2015 – Prague, 1-4/9), J. Kruis, Y. Tsompanakis, B.H.V. Topping (eds.), Civil-Comp Press (Stirlingshire), Paper 36. (full paper in USB Key Drive Proceedings)

Ellobody E, Young B (2005). “Behavior of cold-formed steel plain angle columns”. *Journal of Structural Engineering* (ASCE), **131**(3):457-66.

Kwon YB, Kim BS, Hancock GJ (2009). “Compression tests of high strength cold-formed steel channels with buckling interaction”, *Journal of Constructional Steel Research*, **65**(2), 278-89.

Martins AD, Camotim D, Dinis PB, Young B (2015a). “Local-distortional interaction in cold-formed steel columns: mechanics, testing, numerical simulation and design”, *Structures*, **4**(November), 38-57.

Martins AD, Dinis PB, Camotim D, Providência P (2015b). “On the relevance of local-distortional interaction effects in the behaviour and design of cold-formed steel columns”, *Computers & Structures*, **160**(November), 57-89.

Santos ES, Batista EM, Camotim D (2012). “Experimental investigation concerning lipped channel columns undergoing local-distortional-global buckling mode interaction”, *Thin-Walled Structures*, **54**(May), 19-34.

Santos ES, Batista EM, Camotim D (2014a). “Cold-formed steel columns under L-D-G interaction: experimental investigation”, *Steel Construction*, **7**(3), 193-198.

Santos ES, Dinis PB, Batista EM, Camotim D (2014b). “Cold-formed steel lipped channel columns undergoing local-distortional-global interaction: experimental and numerical investigation”, *Proceedings of 22nd International Specialty Conference on Cold-Formed Steel Structures* (St. Louis, 5-6/11), R. LaBoube, W.-W. Yu (eds.), 193-211.

Schafer BW (2002). “Local, distortional and Euler buckling in thin-walled columns”, *Journal of Structural Engineering* (ASCE), **128**(3), 288-299.

Schafer BW (2008). “Review: the direct strength method of cold-formed steel member design”, *Journal of Constructional Steel Research*, **64**(7-8), 766-778.

Silvestre N, Camotim D, Dinis PB (2012). “Post-buckling behaviour and direct strength design of lipped channel columns experiencing local/distortional interaction”, *Journal of Constructional Steel Research*, **73**(June), 12-30.

Yang D, Hancock GJ (2004). “Compression tests of high strength steel columns with interaction between local and distortional buckling”, *Journal of Structural Engineering* (ASCE), **130**(12), 1954-1963.

Yap DCY, Hancock GJ (2011). “Experimental study of high strength cold-formed stiffened web steel sections”, *Journal of Structural Engineering* (ASCE), **137**(2), 162-172.

Young B, Rasmussen KJR (1998). “Design of lipped channel columns’’ *Journal of Structural Engineering* (ASCE), **124**(2), 140-148.

Young B, Yan J (2002). “Channel columns undergoing local, distortional and overall buckling”, *Journal of Structural Engineering* (ASCE), **128**(6), 728-736.

Young B, Silvestre N, Camotim D (2013a). “Cold-formed steel lipped channel columns influenced by local-distortional interaction: strength and DSM design”, *Journal of Structural Engineering* (ASCE), **139**(6), 1059-1074.

Young B, Camotim D, Dinis PB (2013b). “Tests of cold-formed steel lipped channel columns undergoing local-distortional-global interaction”, *Research and Applications in Structural Engineering, Mechanics and Computation* (SEMC 2013 – Cape Town, 2-4/9), A. Zingoni (Ed.), Taylor & Francis (London), 387-388. (full paper in CD-ROM Proceedings - 1071-1076)

Young B, Dinis, PB, Camotim, D (2015). “L-D-G Interaction in CFS lipped channel columns – part I: experimental investigation”, *Proceedings of 15th International Conference on Civil, Structural and Environmental Engineering Computing* (CC 2015 – Prague, 1-4/9), J. Kruis, Y. Tsompanakis, B.H.V. Topping (eds.), Civil-Comp Press (Stirlingshire), Paper 35. (full paper in USB Key Drive Proceedings)

ANNEX A: FIXED-ENDED COLUMN EXPERIMENTAL FAILURE LOAD DATA

Table A1: University of Hong Kong test failure loads and their DSM estimates (stresses in MPa)

	Test		NLE			NDG		NLDG	
Specimen	f_y	f_{Exp}	λ_E	f_{NLE}		f_{NDG}		f_{NLDG}	
LC1	597	253.0	1.39	221.8	1.14	208.7	1.21	188.6	1.34
LC2-1	597	237.8	1.54	188.0	1.26	174.8	1.36	160.3	1.48
LC2-2	597	222.2	1.52	190.9	1.16	178.1	1.25	162.8	1.37
LC3	597	186.5	1.69	157.8	1.18	145.1	1.28	134.8	1.38
LC4	597	177.2	1.84	131.4	1.35	121.7	1.46	112.0	1.58
LC5	594	225.1	1.56	183.6	1.23	158.4	1.42	149.9	1.50
LC6	594	204.1	1.68	161.6	1.26	137.2	1.49	131.6	1.55
LC7	594	162.4	1.79	141.8	1.14	120.9	1.34	115.7	1.40
LC8	594	149.6	1.89	124.6	1.20	105.4	1.42	99.9	1.50
LC9	597	300.4	1.27	248.0	1.21	243.4	1.23	213.8	1.41
LC10	597	273.1	1.37	218.7	1.25	212.1	1.29	184.8	1.48
LC11	597	206.7	1.54	180.3	1.15	167.8	1.23	149.6	1.38
LC12	597	232.0	1.51	184.5	1.26	178.4	1.30	155.8	1.49
LC13	594	258.8	1.43	213.8	1.21	190.8	1.36	176.5	1.47
LC14	594	224.8	1.53	183.4	1.23	164.6	1.37	150.1	1.50
LC15	594	193.5	1.66	157.7	1.23	137.9	1.40	127.8	1.51
LC16	594	166.7	1.77	141.3	1.18	123.7	1.35	115.8	1.44
				Mean	1.22		1.34		1.46
				S. Dev.	0.05		0.08		0.07
				Min	1.14		1.22		1.34
				Max	1.35		1.50		1.59

Table A2: University of Sydney test failure loads and their DSM estimates (stresses in MPa)

	Test		NLE			NDG		NLDG	
Specimen	f_y	f_{Exp}	λ_E	f_{NLE}		f_{NDG}		f_{NLDG}	
L48F1500	550	316	0.97	276.9	1.14	235.7	1.34	204.7	1.54
L48F2000	550	286	1.21	240.9	1.19	210	1.36	190.3	1.50
				Mean	1.16		1.35		1.52
				S. Dev.	0.03		0.02		0.03
				Min	1.14		1.34		1.50
				Max	1.19		1.36		1.54

Table A3: University of Yeungnam test failure loads and their DSM estimates (stresses in MPa)

	Test		NLE			NDG		NLDG	
Specimen	f_y	f_{Exp}	λ_E	f_{NLE}		f_{NDG}		f_{NLDG}	
A-6-1-1200	628	159	1.56	177.9	0.89	154.1	1.03	137.9	1.15
A-8-1-1200	633	229.5	1.34	237.4	0.97	206.1	1.11	185.3	1.24
A-8-2-800	633	274.5	1.13	301.1	0.91	262.5	1.05	238.1	1.15
A-8-2-1000	633	238.1	1.32	264.4	0.9	234	1.02	220.2	1.08
A-8-2-1200	633	210.8	1.53	222.2	0.95	198.9	1.06	197	1.07
				Mean	0.92		1.05		1.14
				S. Dev.	0.03		0.04		0.07
				Min	0.89		1.02		1.07
				Max	0.97		1.11		1.24

Table A4: COPPE first campaign test failure loads and their DSM estimates (stresses in MPa)

	Test		NLE			NDG		NLDG	
Specimen	f_y	f_{Exp}	λ_E	f_{NLE}		f_{NDG}		f_{NLDG}	
C1	342	114	1.50	119.8	0.95	106.0	1.08	102.5	1.13
C2	342	105	1.50	119.8	0.88	106.0	0.99	102.5	1.04
C3	342	111	1.50	119.6	0.93	105.7	1.05	102.1	1.10
C4	342	131	1.29	152.9	0.86	134.9	0.97	130.5	1.00
C5	342	124	1.29	153.0	0.81	135.0	0.92	130.6	0.94
C6	342	109	1.29	153.0	0.71	135.0	0.81	130.6	0.83
C7	342	148	1.25	163.8	0.90	146.4	1.01	143.4	1.04
C8	342	144	1.25	164.4	0.88	146.9	0.98	144.3	1.01
C9	342	158	1.11	194.0	0.81	172.6	0.92	172.6	0.93
C10	342	152	1.11	193.9	0.78	172.5	0.88	172.5	0.89
C21	407	152	1.40	158.7	0.96	140.2	1.08	134.3	1.14
C22	407	142	1.40	159.1	0.89	140.7	1.01	135.0	1.06
				Mean	0.86		0.97		1.01
				S. Dev.	0.07		0.08		0.09
				Min	0.71		0.81		0.83
				Max	0.96		1.08		1.14

Table A5: COPPE second campaign test failure loads and their DSM estimates (stresses in MPa)

	Test		NLE			NDG		NLDG	
Specimen	f_y	f_{Exp}	λ_E	f_{NLE}		f_{NDG}		f_{NLDG}	
CP2	345	150.7	1.38	137.2	1.10	126.0	1.20	118.7	1.27
CP4	345	147.1	1.36	139.5	1.05	128.2	1.15	120.2	1.22
CP6	345	162.6	1.34	142.7	1.14	130.5	1.25	122.7	1.33
CP8	345	140.9	1.26	150.2	0.94	138.6	1.02	127.4	1.11
CP10	345	155.3	1.22	155.4	1.00	142.4	1.09	130.4	1.19
CP12	345	171.6	1.19	159.0	1.08	146.3	1.17	132.8	1.29
CP14	345	143.6	1.30	151.6	0.95	139.7	1.03	132.9	1.08
CP16	345	144.7	1.28	154.8	0.93	143.4	1.01	136.0	1.06
CP18	345	166.1	1.26	155.0	1.07	144.3	1.15	134.4	1.24
CP20	345	158.5	1.20	162.6	0.97	151.2	1.05	139.6	1.13
CP22	345	180.2	1.17	178.0	1.01	164.5	1.09	158.7	1.14
CP24	345	176.6	1.15	179.6	0.98	166.2	1.06	159.1	1.11
CP26	345	165.8	1.12	182.6	0.91	169.3	0.98	161.2	1.03
CP28	345	183.9	1.05	191.7	0.96	177.6	1.04	167.4	1.10
CP30	345	192.4	1.02	196.9	0.98	182.2	1.06	171.3	1.12
CP32	345	197.1	1.00	197.4	1.00	183.6	1.07	171.4	1.15
				Mean	1.00		1.09		1.16
				S. Dev.	0.07		0.08		0.09
				Min	0.91		0.98		1.03
				Max	1.14		1.25		1.33

ANNEX B: FIXED-ENDED COLUMN NUMERICAL FAILURE DATA

Table B1: LC_N column numerical ultimate strengths and their DSM estimates (stresses in MPa)

	SFEA		NLG			NDG		NLDG	
Column	f_y	f_{Num}	λ_G	f_{NLG}		f_{NDG}		f_{NLDG}	
LC1	300	204	0.99	183.0	1.11	173.5	1.18	166.3	1.23
	500	245	1.27	215.1	1.14	202.9	1.21	185.0	1.32
	700	261	1.51	224.5	1.16	211.2	1.24	190.0	1.37
	900	268	1.71	224.5	1.19	211.2	1.27	190.0	1.41
LC2-1	300	179	1.09	165.0	1.08	154.4	1.16	147.3	1.22
	500	205	1.41	186.2	1.10	173.2	1.18	159.3	1.29
	700	222	1.67	188.0	1.18	174.8	1.27	160.3	1.38
	900	230	1.89	188.0	1.22	174.8	1.32	160.3	1.43
LC2-2	300	181	1.08	166.5	1.09	156.3	1.16	148.9	1.22
	500	207	1.39	188.6	1.10	176.2	1.18	161.5	1.28
	700	217	1.65	190.9	1.14	178.1	1.22	162.8	1.33
	900	227	1.87	190.9	1.19	178.1	1.27	162.8	1.39
LC3	300	157	1.20	146.7	1.07	135.5	1.16	128.6	1.22
	500	175	1.55	157.8	1.11	145.1	1.21	134.8	1.30
	700	186	1.83	157.8	1.18	145.1	1.28	134.8	1.38
	900	193	2.07	157.8	1.22	145.1	1.33	134.8	1.43
LC4	300	136	1.31	127.2	1.07	118.1	1.15	109.7	1.24
	500	153	1.69	131.4	1.16	121.7	1.26	112.0	1.37
	700	164	1.99	131.4	1.25	121.7	1.35	112.0	1.46
	900	177	2.26	131.4	1.35	121.7	1.45	112.0	1.58
LC5	300	169	1.11	163.0	1.04	142.3	1.19	139.3	1.21
	500	201	1.43	182.5	1.10	157.6	1.28	149.4	1.35
	700	217	1.70	183.6	1.18	158.4	1.37	149.9	1.45
	900	230	1.92	183.6	1.25	158.4	1.45	149.9	1.53
LC6	300	154	1.19	149.7	1.03	128.2	1.20	125.6	1.23
	500	185	1.54	161.6	1.15	137.2	1.35	131.6	1.41
	700	203	1.82	161.6	1.26	137.2	1.48	131.6	1.54
	900	216	2.06	161.6	1.34	137.2	1.57	131.6	1.64
LC7	300	140	1.27	135.7	1.03	116.2	1.20	112.6	1.24
	500	166	1.64	141.8	1.17	120.9	1.37	115.7	1.43
	700	181	1.94	141.8	1.28	120.9	1.50	115.7	1.56
	900	165	2.20	141.8	1.16	120.9	1.36	115.7	1.43
LC8	300	128	1.34	121.8	1.05	103.3	1.24	98.6	1.30
	500	148	1.73	124.6	1.19	105.4	1.40	99.9	1.48
	700	165	2.05	124.6	1.32	105.4	1.57	99.9	1.65
	900	174	2.33	124.6	1.40	105.4	1.65	99.9	1.74
LC9	300	227	0.90	195.7	1.16	192.4	1.18	182.3	1.25
	500	285	1.16	237.1	1.20	233.1	1.22	207.7	1.37
	700	301	1.38	255.1	1.18	249.9	1.20	217.7	1.38
	900	307	1.56	259.0	1.19	253.5	1.21	219.7	1.40

	SFEA		NLG			NDG		NLDG	
Column	f_y	f_{Num}	λ_G	f_{NLG}		f_{NDG}		f_{NLDG}	
LC10	300	210	0.97	179.1	1.17	175.0	1.20	162.3	1.29
	500	247	1.25	211.5	1.17	205.6	1.20	181.0	1.36
	700	256	1.48	222.2	1.15	215.2	1.19	186.6	1.37
	900	261	1.68	222.4	1.17	215.4	1.21	186.7	1.40
LC11	300	178	1.09	158.3	1.12	148.7	1.20	137.8	1.29
	500	201	1.41	178.6	1.13	166.3	1.21	148.7	1.35
	700	215	1.66	180.3	1.19	167.8	1.28	149.6	1.44
	900	225	1.89	180.3	1.25	167.8	1.34	149.6	1.50
LC12	300	186	1.07	160.0	1.16	155.9	1.19	142.2	1.31
	500	208	1.38	181.9	1.14	176.1	1.18	154.4	1.35
	700	215	1.63	184.5	1.17	178.4	1.21	155.8	1.38
	900	220	1.85	184.5	1.19	178.4	1.23	155.8	1.41
LC13	300	196	1.01	179.3	1.09	162.0	1.21	157.9	1.24
	500	225	1.31	208.5	1.08	186.5	1.21	173.8	1.29
	700	238	1.55	215.3	1.11	191.9	1.24	177.2	1.34
	900	251	1.76	215.3	1.17	191.9	1.31	177.2	1.42
LC14	300	177	1.09	161.0	1.10	146.1	1.21	138.4	1.28
	500	196	1.41	181.6	1.08	163.2	1.20	149.2	1.31
	700	209	1.66	183.4	1.14	164.6	1.27	150.1	1.39
	900	220	1.89	183.4	1.20	164.6	1.34	150.1	1.47
LC15	300	153	1.18	145.6	1.05	128.4	1.19	121.7	1.26
	500	172	1.53	157.7	1.09	137.9	1.25	127.8	1.35
	700	183	1.81	157.7	1.16	137.9	1.33	127.8	1.43
	900	196	2.05	157.7	1.24	137.9	1.42	127.8	1.53
LC16	300	138	1.26	134.6	1.03	118.5	1.16	112.4	1.23
	500	158	1.62	141.3	1.12	123.7	1.28	115.8	1.36
	700	169	1.92	141.3	1.20	123.7	1.37	115.8	1.46
	900	179	2.18	141.3	1.27	123.7	1.45	115.8	1.55
				Mean	1.16		1.28		1.38
				S. Dev.	0.08		0.11		0.11
				Min	1.03		1.15		1.21
				Max	1.40		1.65		1.74

Table B2: LP_N column dimensions, numerical ultimate strengths and their DSM estimates (mm, MPa)

								SFEA		NLG			NDG		NLDG	
b_w	b_f	b_s	t	L	f_{crL}	f_{crD}	f_{crG}	f_y	f_{Num}	λ_G	f_{NLG}		f_{NDG}		f_{NLDG}	
85	75	12	1.4	2300	241.4	205.6	244.5	300	173	1.11	168.0	1.03	141.9	1.22	141.9	1.22
85	75	12	1.4	2300	241.4	205.6	244.5	450	195	1.36	185.8	1.05	155.4	1.25	152.2	1.28
85	75	12	1.4	2300	241.4	205.6	244.5	600	213	1.57	189.5	1.12	158.1	1.35	154.0	1.38
85	75	12	1.4	2300	241.4	205.6	244.5	750	224	1.75	189.5	1.18	158.1	1.42	154.0	1.45
85	75	12	1.4	2300	241.4	205.6	244.5	900	231	1.92	189.5	1.22	158.1	1.46	154.0	1.50
85	75	12	1.4	2300	241.4	205.6	244.5	1200	245	2.22	189.5	1.29	158.1	1.55	154.0	1.59
85	75	12	1.4	2400	241.3	204.4	230.5	300	168	1.14	164.4	1.02	138.9	1.21	138.9	1.21
85	75	12	1.4	2400	241.3	204.4	230.5	450	190	1.40	180.0	1.06	150.7	1.26	149.0	1.28
85	75	12	1.4	2400	241.3	204.4	230.5	600	207	1.61	182.1	1.14	152.3	1.36	150.1	1.38
85	75	12	1.4	2400	241.3	204.4	230.5	750	217	1.80	182.1	1.19	152.3	1.42	150.1	1.45
85	75	12	1.4	2400	241.3	204.4	230.5	900	224	1.98	182.1	1.23	152.3	1.47	150.1	1.49
85	75	12	1.4	2400	241.3	204.4	230.5	1200	228	2.28	182.1	1.25	152.3	1.50	150.1	1.52
85	75	12	1.4	2500	241.3	203.8	216.9	300	163	1.18	160.6	1.01	135.8	1.20	135.8	1.20
85	75	12	1.4	2500	241.3	203.8	216.9	450	185	1.44	173.8	1.06	146.0	1.27	145.7	1.27
85	75	12	1.4	2500	241.3	203.8	216.9	600	201	1.66	174.7	1.15	146.6	1.37	146.2	1.37
85	75	12	1.4	2500	241.3	203.8	216.9	750	211	1.86	174.7	1.21	146.6	1.44	146.2	1.44
85	75	12	1.4	2500	241.3	203.8	216.9	900	217	2.04	174.7	1.24	146.6	1.48	146.2	1.48
85	75	12	1.4	2500	241.3	203.8	216.9	1200	220	2.35	174.7	1.26	146.6	1.50	146.2	1.50
85	75	12	1.4	2600	241.3	203.7	204.1	300	158	1.21	156.7	1.01	132.6	1.19	132.6	1.19
85	75	12	1.4	2600	241.3	203.7	204.1	450	180	1.48	167.5	1.07	141.1	1.28	141.1	1.28
85	75	12	1.4	2600	241.3	203.7	204.1	600	196	1.71	167.6	1.17	141.2	1.39	141.2	1.39
85	75	12	1.4	2600	241.3	203.7	204.1	750	205	1.92	167.6	1.22	141.2	1.45	141.2	1.45
85	75	12	1.4	2600	241.3	203.7	204.1	900	211	2.10	167.6	1.26	141.2	1.49	141.2	1.49
85	75	12	1.4	2600	241.3	203.7	204.1	1200	222	2.42	167.6	1.32	141.2	1.57	141.2	1.57
85	75	12	1.4	2700	241.3	202.5	191.9	300	152	1.25	152.5	1.00	129.1	1.18	129.1	1.18
85	75	12	1.4	2700	241.3	202.5	191.9	450	175	1.53	160.7	1.09	135.5	1.29	135.5	1.29
85	75	12	1.4	2700	241.3	202.5	191.9	600	191	1.77	160.7	1.19	135.5	1.41	135.5	1.41
85	75	12	1.4	2700	241.3	202.5	191.9	750	200	1.98	160.7	1.24	135.5	1.48	135.5	1.48
85	75	12	1.4	2700	241.3	202.5	191.9	900	205	2.17	160.7	1.28	135.5	1.51	135.5	1.51
85	75	12	1.4	2700	241.3	202.5	191.9	1200	200	2.50	160.7	1.24	135.5	1.48	135.5	1.48
80	75	12	1.2	2400	191.1	178.3	202.9	300	150	1.22	145.1	1.03	125.9	1.19	122.4	1.23
80	75	12	1.2	2400	191.1	178.3	202.9	450	169	1.49	154.8	1.09	133.5	1.27	127.4	1.33
80	75	12	1.2	2400	191.1	178.3	202.9	600	180	1.72	154.8	1.16	133.6	1.35	127.5	1.41
80	75	12	1.2	2400	191.1	178.3	202.9	750	188	1.92	154.8	1.21	133.6	1.41	127.5	1.48
80	75	12	1.2	2400	191.1	178.3	202.9	900	196	2.11	154.8	1.27	133.6	1.47	127.5	1.54
80	75	12	1.2	2400	191.1	178.3	202.9	1200	210	2.43	154.8	1.36	133.6	1.57	127.5	1.65
80	75	12	1.2	2500	191.1	176.9	191.6	300	145	1.25	141.5	1.02	122.8	1.18	120.3	1.21
80	75	12	1.2	2500	191.1	176.9	191.6	450	165	1.53	149.0	1.11	128.6	1.28	124.2	1.33
80	75	12	1.2	2500	191.1	176.9	191.6	600	175	1.77	149.0	1.17	128.6	1.36	124.2	1.41
80	75	12	1.2	2500	191.1	176.9	191.6	750	183	1.98	149.0	1.23	128.6	1.42	124.2	1.47
80	75	12	1.2	2500	191.1	176.9	191.6	900	189	2.17	149.0	1.27	128.6	1.47	124.2	1.52
80	75	12	1.2	2500	191.1	176.9	191.6	1200	203	2.50	149.0	1.36	128.6	1.58	124.2	1.63

								SFEA		NLG			NDG		NLDG	
b_w	b_f	b_s	t	L	f_{crL}	f_{crD}	f_{crG}	f_y	f_{Num}	λ_G	f_{NLG}		f_{NDG}		f_{NLDG}	
80	75	12	1.2	2600	191.0	176.1	180.7	300	140	1.29	137.8	1.02	119.6	1.17	118.1	1.19
80	75	12	1.2	2600	191.0	176.1	180.7	450	161	1.58	143.2	1.12	123.9	1.30	121.0	1.33
80	75	12	1.2	2600	191.0	176.1	180.7	600	170	1.82	143.2	1.19	123.9	1.37	121.0	1.40
80	75	12	1.2	2600	191.0	176.1	180.7	750	177	2.04	143.2	1.24	123.9	1.43	121.0	1.46
80	75	12	1.2	2600	191.0	176.1	180.7	900	184	2.23	143.2	1.29	123.9	1.49	121.0	1.52
80	75	12	1.2	2600	191.0	176.1	180.7	1200	196	2.58	143.2	1.37	123.9	1.58	121.0	1.62
80	75	12	1.2	2700	191.0	175.8	170.3	300	135	1.33	133.8	1.01	116.3	1.16	115.9	1.16
80	75	12	1.2	2700	191.0	175.8	170.3	450	157	1.63	137.5	1.14	119.3	1.32	117.9	1.33
80	75	12	1.2	2700	191.0	175.8	170.3	600	166	1.88	137.5	1.21	119.3	1.39	117.9	1.41
80	75	12	1.2	2700	191.0	175.8	170.3	750	173	2.10	137.5	1.26	119.3	1.45	117.9	1.47
80	75	12	1.2	2700	191.0	175.8	170.3	900	186	2.30	137.5	1.35	119.3	1.56	117.9	1.58
80	75	12	1.2	2700	191.0	175.8	170.3	1200	193	2.65	137.5	1.40	119.3	1.62	117.9	1.64
80	75	12	1.2	2800	191.0	175.7	160.5	300	131	1.37	129.8	1.01	113.0	1.16	113.0	1.16
80	75	12	1.2	2800	191.0	175.7	160.5	450	153	1.67	132.1	1.16	114.9	1.33	114.9	1.33
80	75	12	1.2	2800	191.0	175.7	160.5	600	161	1.93	132.1	1.22	114.9	1.40	114.9	1.40
80	75	12	1.2	2800	191.0	175.7	160.5	750	168	2.16	132.1	1.27	114.9	1.46	114.9	1.46
80	75	12	1.2	2800	191.0	175.7	160.5	900	180	2.37	132.1	1.36	114.9	1.57	114.9	1.57
80	75	12	1.2	2800	191.0	175.7	160.5	1200	187	2.73	132.1	1.42	114.9	1.63	114.9	1.63
90	74	13	1.5	2350	257.9	236.7	269.4	300	189	1.06	177.2	1.07	154.0	1.23	154.0	1.23
90	74	13	1.5	2350	257.9	236.7	269.4	450	206	1.29	199.2	1.03	171.5	1.20	166.3	1.24
90	74	13	1.5	2350	257.9	236.7	269.4	600	225	1.49	206.6	1.09	177.3	1.27	170.1	1.32
90	74	13	1.5	2350	257.9	236.7	269.4	750	238	1.67	206.7	1.15	177.3	1.34	170.1	1.40
90	74	13	1.5	2350	257.9	236.7	269.4	900	247	1.83	206.7	1.20	177.3	1.39	170.1	1.45
90	74	13	1.5	2350	257.9	236.7	269.4	1200	249	2.11	206.7	1.20	177.3	1.40	170.1	1.46
90	74	13	1.5	2400	257.9	235.9	261.2	300	187	1.07	175.4	1.07	152.4	1.23	152.4	1.23
90	74	13	1.5	2400	257.9	235.9	261.2	450	203	1.31	196.2	1.03	169.0	1.20	164.6	1.23
90	74	13	1.5	2400	257.9	235.9	261.2	600	222	1.52	202.4	1.10	173.8	1.28	167.8	1.32
90	74	13	1.5	2400	257.9	235.9	261.2	750	234	1.69	202.4	1.16	173.8	1.35	167.8	1.39
90	74	13	1.5	2400	257.9	235.9	261.2	900	243	1.86	202.4	1.20	173.8	1.40	167.8	1.45
90	74	13	1.5	2400	257.9	235.9	261.2	1200	240	2.14	202.4	1.19	173.8	1.38	167.8	1.43
90	74	13	1.5	2500	257.9	234.9	245.4	300	181	1.11	171.7	1.05	149.2	1.21	149.2	1.21
90	74	13	1.5	2500	257.9	234.9	245.4	450	197	1.35	190.2	1.04	164.0	1.20	161.2	1.22
90	74	13	1.5	2500	257.9	234.9	245.4	600	216	1.56	194.0	1.11	167.0	1.29	163.3	1.32
90	74	13	1.5	2500	257.9	234.9	245.4	750	227	1.75	194.0	1.17	167.0	1.36	163.3	1.39
90	74	13	1.5	2500	257.9	234.9	245.4	900	236	1.92	194.0	1.22	167.0	1.41	163.3	1.45
90	74	13	1.5	2500	257.9	234.9	245.4	1200	238	2.21	194.0	1.23	167.0	1.42	163.3	1.46
90	74	13	1.5	2600	257.9	234.5	230.5	300	175	1.14	167.9	1.04	145.9	1.20	145.9	1.20
90	74	13	1.5	2600	257.9	234.5	230.5	450	191	1.40	183.8	1.04	158.9	1.20	157.7	1.21
90	74	13	1.5	2600	257.9	234.5	230.5	600	210	1.61	186.0	1.13	160.6	1.31	158.9	1.32
90	74	13	1.5	2600	257.9	234.5	230.5	750	221	1.80	186.0	1.19	160.6	1.38	158.9	1.39
90	74	13	1.5	2600	257.9	234.5	230.5	900	229	1.98	186.0	1.23	160.6	1.43	158.9	1.44
90	74	13	1.5	2600	257.9	234.5	230.5	1200	252	2.28	186.0	1.36	160.6	1.57	158.9	1.59
90	74	13	1.5	2700	257.8	234.2	216.5	300	169	1.18	163.9	1.03	142.5	1.19	142.5	1.19
90	74	13	1.5	2700	257.8	234.2	216.5	450	186	1.44	177.4	1.05	153.6	1.21	153.6	1.21
90	74	13	1.5	2700	257.8	234.2	216.5	600	205	1.66	178.2	1.15	154.3	1.33	154.3	1.33
90	74	13	1.5	2700	257.8	234.2	216.5	750	215	1.86	178.2	1.21	154.3	1.39	154.3	1.39
90	74	13	1.5	2700	257.8	234.2	216.5	900	222	2.04	178.2	1.25	154.3	1.44	154.3	1.44
90	74	13	1.5	2700	257.8	234.2	216.5	1200	231	2.35	178.2	1.30	154.3	1.50	154.3	1.50

								SFEA		NLG			NDG		NLDG	
b_w	b_f	b_s	t	L	f_{crL}	f_{crD}	f_{crG}	f_y	f_{Num}	λ_G	f_{NLG}		f_{NDG}		f_{NLDG}	
110	67	12	2.0	2500	330.2	312.6	337.7	300	225	0.94	204.3	1.10	180.1	1.25	180.1	1.25
110	67	12	2.0	2500	330.2	312.6	337.7	450	263	1.15	237.4	1.11	208.1	1.26	205.2	1.28
110	67	12	2.0	2500	330.2	312.6	337.7	600	274	1.33	254.3	1.08	221.8	1.24	214.3	1.28
110	67	12	2.0	2500	330.2	312.6	337.7	750	283	1.49	260.8	1.09	226.9	1.25	217.7	1.30
110	67	12	2.0	2500	330.2	312.6	337.7	900	294	1.63	260.9	1.13	226.9	1.30	217.7	1.35
110	67	12	2.0	2500	330.2	312.6	337.7	1200	310	1.88	260.9	1.19	226.9	1.37	217.7	1.42
110	67	12	2.0	2600	330.2	312.2	315.6	300	219	0.98	200.7	1.09	176.9	1.24	176.9	1.24
110	67	12	2.0	2600	330.2	312.2	315.6	450	254	1.19	231.2	1.10	202.9	1.25	201.6	1.26
110	67	12	2.0	2600	330.2	312.2	315.6	600	264	1.38	245.5	1.08	214.6	1.23	209.5	1.26
110	67	12	2.0	2600	330.2	312.2	315.6	750	275	1.54	249.2	1.10	217.6	1.26	211.5	1.30
110	67	12	2.0	2600	330.2	312.2	315.6	900	285	1.69	249.2	1.14	217.6	1.31	211.5	1.35
110	67	12	2.0	2600	330.2	312.2	315.6	1200	299	1.95	249.2	1.20	217.6	1.37	211.5	1.41
110	67	12	2.0	2700	330.1	310.7	295.4	300	213	1.01	196.1	1.09	173.3	1.23	173.3	1.23
110	67	12	2.0	2700	330.1	310.7	295.4	450	244	1.23	224.8	1.09	197.3	1.24	197.3	1.24
110	67	12	2.0	2700	330.1	310.7	295.4	600	254	1.43	236.6	1.07	207.0	1.23	204.4	1.24
110	67	12	2.0	2700	330.1	310.7	295.4	750	267	1.59	238.3	1.12	208.4	1.28	205.3	1.30
110	67	12	2.0	2700	330.1	310.7	295.4	900	276	1.75	238.3	1.16	208.4	1.32	205.3	1.34
110	67	12	2.0	2700	330.1	310.7	295.4	1200	289	2.02	238.3	1.21	208.4	1.39	205.3	1.41
100	60	12	2.0	2400	400.8	381.2	318.7	300	226	0.97	202.3	1.12	187.7	1.20	187.7	1.20
100	60	12	2.0	2400	400.8	381.2	318.7	450	265	1.19	246.7	1.07	217.8	1.22	217.8	1.22
100	60	12	2.0	2400	400.8	381.2	318.7	600	279	1.37	262.6	1.06	231.6	1.20	231.6	1.20
100	60	12	2.0	2400	400.8	381.2	318.7	750	288	1.53	266.9	1.08	235.3	1.22	235.3	1.22
100	60	12	2.0	2400	400.8	381.2	318.7	900	303	1.68	266.9	1.14	235.3	1.29	235.3	1.29
100	60	12	2.0	2400	400.8	381.2	318.7	1200	316	1.94	266.9	1.18	235.3	1.34	235.3	1.34
62	55	11	1.1	1550	280.6	276.4	303.8	300	204	0.99	188.7	1.08	168.3	1.21	168.3	1.21
62	55	11	1.1	1550	280.6	276.4	303.8	450	233	1.22	215.9	1.08	191.2	1.22	183.9	1.27
62	55	11	1.1	1550	280.6	276.4	303.8	600	246	1.41	228.1	1.08	200.9	1.22	190.3	1.29
62	55	11	1.1	1550	280.6	276.4	303.8	750	256	1.57	230.3	1.11	202.8	1.26	191.5	1.34
62	55	11	1.1	1550	280.6	276.4	303.8	900	265	1.72	230.3	1.15	202.8	1.31	191.5	1.38
62	55	11	1.1	1550	280.6	276.4	303.8	1200	280	1.99	230.3	1.22	202.8	1.38	191.5	1.46
62	55	11	1.1	1600	280.5	275.6	291.1	300	200	1.02	186.3	1.07	166.1	1.20	166.1	1.20
62	55	11	1.1	1600	280.5	275.6	291.1	450	227	1.24	212.0	1.07	187.8	1.21	181.6	1.25
62	55	11	1.1	1600	280.5	275.6	291.1	600	241	1.44	222.6	1.08	196.4	1.23	187.3	1.29
62	55	11	1.1	1600	280.5	275.6	291.1	750	251	1.61	223.8	1.12	197.3	1.27	187.9	1.34
62	55	11	1.1	1600	280.5	275.6	291.1	900	259	1.76	223.8	1.16	197.3	1.31	187.9	1.38
62	55	11	1.1	1600	280.5	275.6	291.1	1200	274	2.03	223.8	1.22	197.3	1.39	187.9	1.46
62	55	11	1.1	1700	280.5	275.1	266.5	300	192	1.06	181.3	1.06	161.6	1.19	161.6	1.19
62	55	11	1.1	1700	280.5	275.1	266.5	450	215	1.30	203.6	1.06	180.7	1.19	176.9	1.22
62	55	11	1.1	1700	280.5	275.1	266.5	600	231	1.50	210.8	1.10	186.7	1.24	180.9	1.28
62	55	11	1.1	1700	280.5	275.1	266.5	750	242	1.68	210.8	1.15	186.7	1.30	180.9	1.34
62	55	11	1.1	1700	280.5	275.1	266.5	900	249	1.84	210.8	1.18	186.7	1.33	180.9	1.38
62	55	11	1.1	1700	280.5	275.1	266.5	1200	263	2.12	210.8	1.25	186.7	1.41	180.9	1.45
62	55	11	1.1	1800	280.5	270.9	243.6	300	183	1.11	175.9	1.04	156.0	1.17	156.0	1.17
62	55	11	1.1	1800	280.5	270.9	243.6	450	202	1.36	194.6	1.04	172.2	1.17	171.1	1.18
62	55	11	1.1	1800	280.5	270.9	243.6	600	222	1.57	198.4	1.12	175.3	1.27	173.3	1.28
62	55	11	1.1	1800	280.5	270.9	243.6	750	232	1.75	198.4	1.17	175.3	1.32	173.3	1.34
62	55	11	1.1	1800	280.5	270.9	243.6	900	238	1.92	198.4	1.20	175.3	1.36	173.3	1.37
62	55	11	1.1	1800	280.5	270.9	243.6	1200	247	2.22	198.4	1.25	175.3	1.41	173.3	1.43

								SFEA		NLG			NDG		NLDG	
b_w	b_f	b_s	t	L	f_{crL}	f_{crD}	f_{crG}	f_y	f_{Num}	λ_G	f_{NLG}		f_{NDG}		f_{NLDG}	
62	55	11	1.1	1900	280.4	267.4	222.8	300	174	1.16	170.1	1.02	150.4	1.16	150.4	1.16
62	55	11	1.1	1900	280.4	267.4	222.8	450	190	1.42	185.2	1.03	163.5	1.16	163.5	1.16
62	55	11	1.1	1900	280.4	267.4	222.8	600	213	1.64	186.7	1.14	164.7	1.29	164.7	1.29
62	55	11	1.1	1900	280.4	267.4	222.8	750	222	1.83	186.7	1.19	164.7	1.35	164.7	1.35
62	55	11	1.1	1900	280.4	267.4	222.8	900	228	2.01	186.7	1.22	164.7	1.38	164.7	1.38
62	55	11	1.1	1900	280.4	267.4	222.8	1200	239	2.32	186.7	1.28	164.7	1.45	164.7	1.45
92	54	11	1.7	2000	344.1	357.6	372.9	300	236	0.90	212.0	1.11	192.3	1.23	192.3	1.23
92	54	11	1.7	2000	344.1	357.6	372.9	450	286	1.10	249.3	1.15	225.8	1.27	219.8	1.30
92	54	11	1.7	2000	344.1	357.6	372.9	600	302	1.27	270.3	1.12	243.7	1.24	231.6	1.30
92	54	11	1.7	2000	344.1	357.6	372.9	750	309	1.42	280.4	1.10	252.2	1.23	237.1	1.30
92	54	11	1.7	2000	344.1	357.6	372.9	900	312	1.55	282.7	1.10	254.0	1.23	238.2	1.31
92	54	11	1.7	2000	344.1	357.6	372.9	1200	327	1.79	282.7	1.16	254.0	1.29	238.2	1.37
92	54	11	1.7	2100	344.1	356.3	342.5	300	230	0.94	207.7	1.11	188.0	1.22	188.0	1.22
92	54	11	1.7	2100	344.1	356.3	342.5	450	273	1.15	241.8	1.13	219.0	1.25	215.3	1.27
92	54	11	1.7	2100	344.1	356.3	342.5	600	287	1.32	259.6	1.11	234.4	1.22	225.5	1.27
92	54	11	1.7	2100	344.1	356.3	342.5	750	293	1.48	266.6	1.10	240.4	1.22	229.4	1.28
92	54	11	1.7	2100	344.1	356.3	342.5	900	300	1.62	266.9	1.12	240.6	1.25	229.6	1.31
92	54	11	1.7	2100	344.1	356.3	342.5	1200	313	1.87	266.9	1.17	240.6	1.30	229.6	1.36
92	54	11	1.7	2200	344.1	355.9	315.5	300	222	0.98	201.5	1.10	183.8	1.21	183.8	1.21
92	54	11	1.7	2200	344.1	355.9	315.5	450	259	1.19	234.2	1.11	212.2	1.22	210.6	1.23
92	54	11	1.7	2200	344.1	355.9	315.5	600	272	1.38	248.7	1.09	225.0	1.21	219.3	1.24
92	54	11	1.7	2200	344.1	355.9	315.5	750	279	1.54	252.5	1.11	228.2	1.22	221.4	1.26
92	54	11	1.7	2200	344.1	355.9	315.5	900	288	1.69	252.5	1.14	228.2	1.26	221.4	1.30
92	54	11	1.7	2200	344.1	355.9	315.5	1200	299	1.95	252.5	1.18	228.2	1.31	221.4	1.35
92	54	11	1.7	2300	344.0	354.4	291.5	300	215	1.01	195.0	1.10	179.2	1.20	179.2	1.20
92	54	11	1.7	2300	344.0	354.4	291.5	450	247	1.24	226.4	1.09	205.0	1.20	205.0	1.20
92	54	11	1.7	2300	344.0	354.4	291.5	600	258	1.43	237.9	1.08	215.2	1.20	212.6	1.21
92	54	11	1.7	2300	344.0	354.4	291.5	750	268	1.60	239.2	1.12	216.4	1.24	213.5	1.26
92	54	11	1.7	2300	344.0	354.4	291.5	900	277	1.76	239.2	1.16	216.4	1.28	213.5	1.30
92	54	11	1.7	2300	344.0	354.4	291.5	1200	287	2.03	239.2	1.20	216.4	1.33	213.5	1.34
92	54	11	1.7	2350	344.0	353.6	280.5	300	211	1.03	191.7	1.10	176.9	1.19	176.9	1.19
92	54	11	1.7	2350	344.0	353.6	280.5	450	240	1.27	222.5	1.08	201.3	1.19	201.3	1.19
92	54	11	1.7	2350	344.0	353.6	280.5	600	252	1.46	232.5	1.08	210.2	1.20	209.3	1.20
92	54	11	1.7	2350	344.0	353.6	280.5	750	263	1.64	233.0	1.13	210.8	1.25	209.6	1.25
92	54	11	1.7	2350	344.0	353.6	280.5	900	271	1.79	233.0	1.16	210.8	1.29	209.6	1.29
92	54	11	1.7	2350	344.0	353.6	280.5	1200	281	2.07	233.0	1.21	210.8	1.33	209.6	1.34
75	60	10	1.0	2350	168.2	177.7	189.3	300	145	1.26	135.1	1.07	122.4	1.18	115.3	1.26
75	60	10	1.0	2350	168.2	177.7	189.3	450	156	1.54	141.8	1.10	127.9	1.22	118.8	1.31
75	60	10	1.0	2350	168.2	177.7	189.3	600	166	1.78	141.8	1.17	127.9	1.30	118.8	1.40
75	60	10	1.0	2350	168.2	177.7	189.3	750	170	1.99	141.8	1.20	127.9	1.33	118.8	1.43
75	60	10	1.0	2350	168.2	177.7	189.3	900	178	2.18	141.8	1.26	127.9	1.39	118.8	1.50
75	60	10	1.0	2350	168.2	177.7	189.3	1200	173	2.52	141.8	1.22	127.9	1.35	118.8	1.46
75	60	10	1.0	2400	168.2	176.9	183.0	300	142	1.28	133.0	1.07	120.4	1.18	114.1	1.25
75	60	10	1.0	2400	168.2	176.9	183.0	450	154	1.57	138.5	1.11	125.0	1.23	117.0	1.32
75	60	10	1.0	2400	168.2	176.9	183.0	600	163	1.81	138.5	1.18	125.0	1.30	117.0	1.39
75	60	10	1.0	2400	168.2	176.9	183.0	750	167	2.02	138.5	1.21	125.0	1.34	117.0	1.43
75	60	10	1.0	2400	168.2	176.9	183.0	900	171	2.22	138.5	1.23	125.0	1.37	117.0	1.46
75	60	10	1.0	2400	168.2	176.9	183.0	1200	181	2.56	138.5	1.31	125.0	1.45	117.0	1.55

								SFEA		NLG			NDG		NLDG	
b_w	b_f	b_s	t	L	f_{crL}	f_{crD}	f_{crG}	f_y	f_{Num}	λ_G	f_{NLG}		f_{NDG}		f_{NLDG}	
75	60	10	1.0	2600	168.2	174.9	159.8	300	131	1.37	124.4	1.05	112.6	1.16	108.9	1.20
75	60	10	1.0	2600	168.2	174.9	159.8	450	146	1.68	126.4	1.15	114.4	1.28	110.1	1.33
75	60	10	1.0	2600	168.2	174.9	159.8	600	154	1.94	126.4	1.22	114.4	1.35	110.1	1.40
75	60	10	1.0	2600	168.2	174.9	159.8	750	155	2.17	126.4	1.23	114.4	1.36	110.1	1.41
75	60	10	1.0	2600	168.2	174.9	159.8	900	160	2.37	126.4	1.27	114.4	1.40	110.1	1.45
75	60	10	1.0	2600	168.2	174.9	159.8	1200	160	2.74	126.4	1.27	114.4	1.40	110.1	1.45
75	60	10	1.0	2650	168.2	174.7	154.6	300	129	1.39	122.1	1.06	110.6	1.17	107.6	1.20
75	60	10	1.0	2650	168.2	174.7	154.6	450	144	1.71	123.6	1.16	111.9	1.29	108.5	1.33
75	60	10	1.0	2650	168.2	174.7	154.6	600	151	1.97	123.6	1.22	111.9	1.35	108.5	1.39
75	60	10	1.0	2650	168.2	174.7	154.6	750	156	2.20	123.6	1.26	111.9	1.39	108.5	1.44
75	60	10	1.0	2650	168.2	174.7	154.6	900	165	2.41	123.6	1.33	111.9	1.47	108.5	1.52
75	60	10	1.0	2650	168.2	174.7	154.6	1200	178	2.79	123.6	1.44	111.9	1.59	108.5	1.64
65	47	10	1.1	1550	279.5	306.9	331.7	300	218	0.95	193.0	1.13	178.3	1.22	175.1	1.25
65	47	10	1.1	1550	279.5	306.9	331.7	450	253	1.16	223.4	1.13	205.4	1.23	192.9	1.31
65	47	10	1.1	1550	279.5	306.9	331.7	600	266	1.34	238.7	1.11	218.4	1.22	201.1	1.32
65	47	10	1.1	1550	279.5	306.9	331.7	750	272	1.50	244.0	1.11	222.9	1.22	203.9	1.33
65	47	10	1.1	1550	279.5	306.9	331.7	900	278	1.65	244.0	1.14	222.9	1.25	203.9	1.36
65	47	10	1.1	1550	279.5	306.9	331.7	1200	280	1.90	244.0	1.15	222.9	1.26	203.9	1.37
65	47	10	1.1	1600	279.4	304.7	315.5	300	214	0.98	190.4	1.12	175.5	1.22	173.2	1.24
65	47	10	1.1	1600	279.4	304.7	315.5	450	246	1.19	219.0	1.12	201.1	1.22	190.1	1.29
65	47	10	1.1	1600	279.4	304.7	315.5	600	257	1.38	232.5	1.11	212.6	1.21	197.5	1.30
65	47	10	1.1	1600	279.4	304.7	315.5	750	263	1.54	235.9	1.11	215.5	1.22	199.3	1.32
65	47	10	1.1	1600	279.4	304.7	315.5	900	272	1.69	235.9	1.15	215.5	1.26	199.3	1.36
65	47	10	1.1	1600	279.4	304.7	315.5	1200	285	1.95	235.9	1.21	215.5	1.32	199.3	1.43
65	47	10	1.1	1700	279.4	302.0	285.5	300	205	1.03	185.0	1.11	170.1	1.21	169.5	1.21
65	47	10	1.1	1700	279.4	302.0	285.5	450	231	1.26	209.9	1.10	192.5	1.20	184.6	1.25
65	47	10	1.1	1700	279.4	302.0	285.5	600	240	1.45	219.8	1.09	201.1	1.19	190.1	1.26
65	47	10	1.1	1700	279.4	302.0	285.5	750	249	1.62	220.6	1.13	201.8	1.23	190.6	1.31
65	47	10	1.1	1700	279.4	302.0	285.5	900	258	1.78	220.6	1.17	201.8	1.28	190.6	1.35
65	47	10	1.1	1700	279.4	302.0	285.5	1200	270	2.05	220.6	1.22	201.8	1.34	190.6	1.42
65	47	10	1.1	1800	279.4	301.1	258.9	300	195	1.08	179.4	1.09	164.6	1.18	164.6	1.18
65	47	10	1.1	1800	279.4	301.1	258.9	450	217	1.32	200.5	1.08	184.0	1.18	178.9	1.21
65	47	10	1.1	1800	279.4	301.1	258.9	600	226	1.52	206.5	1.09	189.3	1.19	182.4	1.24
65	47	10	1.1	1800	279.4	301.1	258.9	750	238	1.70	206.5	1.15	189.3	1.26	182.4	1.30
65	47	10	1.1	1800	279.4	301.1	258.9	900	246	1.86	206.5	1.19	189.3	1.30	182.4	1.35
65	47	10	1.1	1800	279.4	301.1	258.9	1200	259	2.15	206.5	1.25	189.3	1.37	182.4	1.42
65	47	10	1.1	1850	279.4	301.1	246.8	300	189	1.10	176.5	1.07	161.9	1.17	161.9	1.17
65	47	10	1.1	1850	279.4	301.1	246.8	450	210	1.35	195.7	1.07	179.7	1.17	176.0	1.19
65	47	10	1.1	1850	279.4	301.1	246.8	600	222	1.56	199.9	1.11	183.4	1.21	178.5	1.24
65	47	10	1.1	1850	279.4	301.1	246.8	750	233	1.74	199.9	1.17	183.4	1.27	178.5	1.31
65	47	10	1.1	1850	279.4	301.1	246.8	900	240	1.91	199.9	1.20	183.4	1.31	178.5	1.34
65	47	10	1.1	1850	279.4	301.1	246.8	1200	257	2.20	199.9	1.29	183.4	1.40	178.5	1.44
80	45	11	1.6	1550	405.2	457.6	478.5	300	258	0.79	230.8	1.12	216.8	1.19	216.8	1.19
80	45	11	1.6	1550	405.2	457.6	478.5	450	333	0.97	283.4	1.18	264.1	1.26	257.6	1.29
80	45	11	1.6	1550	405.2	457.6	478.5	600	370	1.12	315.1	1.17	293.0	1.26	276.6	1.34
80	45	11	1.6	1550	405.2	457.6	478.5	750	384	1.25	335.2	1.15	310.7	1.24	287.9	1.33
80	45	11	1.6	1550	405.2	457.6	478.5	900	390	1.37	346.9	1.12	320.8	1.22	294.2	1.33
80	45	11	1.6	1550	405.2	457.6	478.5	1200	395	1.58	352.6	1.12	325.6	1.21	297.2	1.33

								SFEA		NLG			NDG		NLDG	
b_w	b_f	b_s	t	L	f_{crL}	f_{crD}	f_{crG}	f_y	f_{Num}	λ_G	f_{NLG}		f_{NDG}		f_{NLDG}	
80	45	11	1.6	1600	405.1	457.1	452.8	300	255	0.81	227.4	1.12	214.3	1.19	214.3	1.19
80	45	11	1.6	1600	405.1	457.1	452.8	450	326	1.00	279.1	1.17	260.1	1.25	254.9	1.28
80	45	11	1.6	1600	405.1	457.1	452.8	600	359	1.15	308.8	1.16	287.3	1.25	272.9	1.32
80	45	11	1.6	1600	405.1	457.1	452.8	750	371	1.29	326.9	1.13	303.4	1.22	283.2	1.31
80	45	11	1.6	1600	405.1	457.1	452.8	900	377	1.41	336.7	1.12	311.9	1.21	288.6	1.31
80	45	11	1.6	1600	405.1	457.1	452.8	1200	382	1.63	339.8	1.12	314.6	1.21	290.3	1.32
80	45	11	1.6	1700	405.0	456.9	407.1	300	248	0.86	220.4	1.13	209.2	1.19	209.2	1.19
80	45	11	1.6	1700	405.0	456.9	407.1	450	310	1.05	270.3	1.15	251.7	1.23	249.2	1.24
80	45	11	1.6	1700	405.0	456.9	407.1	600	336	1.21	296.0	1.14	275.7	1.22	265.3	1.27
80	45	11	1.6	1700	405.0	456.9	407.1	750	346	1.36	310.2	1.12	288.5	1.20	273.7	1.26
80	45	11	1.6	1700	405.0	456.9	407.1	900	351	1.49	316.1	1.11	293.8	1.19	277.1	1.27
80	45	11	1.6	1700	405.0	456.9	407.1	1200	359	1.72	316.2	1.14	294.0	1.22	277.2	1.30
80	45	11	1.6	1750	405.0	456.5	386.6	300	244	0.88	216.8	1.13	206.5	1.18	206.5	1.18
80	45	11	1.6	1750	405.0	456.5	386.6	450	301	1.08	265.8	1.13	247.4	1.22	246.2	1.22
80	45	11	1.6	1750	405.0	456.5	386.6	600	325	1.25	289.5	1.12	269.7	1.21	261.3	1.24
80	45	11	1.6	1750	405.0	456.5	386.6	750	334	1.39	301.7	1.11	280.8	1.19	268.7	1.24
80	45	11	1.6	1750	405.0	456.5	386.6	900	339	1.53	305.4	1.11	284.2	1.19	270.9	1.25
80	45	11	1.6	1750	405.0	456.5	386.6	1200	350	1.76	305.4	1.15	284.2	1.23	270.9	1.29
80	45	11	1.6	1800	405.0	453.7	367.7	300	240	0.90	213.2	1.13	203.5	1.18	203.5	1.18
80	45	11	1.6	1800	405.0	453.7	367.7	450	293	1.11	261.3	1.12	242.6	1.21	242.6	1.21
80	45	11	1.6	1800	405.0	453.7	367.7	600	314	1.28	283.0	1.11	263.1	1.19	256.9	1.22
80	45	11	1.6	1800	405.0	453.7	367.7	750	323	1.43	293.3	1.10	272.6	1.19	263.2	1.23
80	45	11	1.6	1800	405.0	453.7	367.7	900	327	1.56	295.2	1.11	274.3	1.19	264.4	1.24
80	45	11	1.6	1800	405.0	453.7	367.7	1200	341	1.81	295.2	1.16	274.3	1.24	264.4	1.29
											Mean	1.15		1.29		1.33
											S. Dev.	0.08		0.10		0.11
											Min	1.00		1.16		1.16
											Max	1.44		1.63		1.65